Very shallow melting of oceanic crust during spreading ridge subduction: Origin of near-trench Quaternary volcanism at the Chile Triple Junction

C. Guivel, Y. Lagabrielle, Jacques Bourgois, H. Martin, N. Arnaud, S. Fourcade, Joseph Cotten, Maury Rc.

Very shallow melting of oceanic crust during spreading ridge subduction: Origin of near-trench Quaternary volcanism at the Chile Triple Junction

Christèle Guivel,[1] Yves Lagabrielle,[2] Jacques Bourgois,[3] Hervé Martin,[4] Nicolas Arnaud,[4] Serge Fourcade,[5] Joseph Cotten,[2] and René C. Maury[2]

Received 29 July 2002; revised 14 March 2003; accepted 1 April 2003; published 25 July 2003.

[1] Recent dacites and basaltic andesites carrying a subduction-related geochemical imprint were dredged within the active Chile Trench off the Taitao Peninsula, where the Chile Ridge is being subducted beneath the South America Plate. Their maximal Ar/Ar ages range from 70–127 ka to 2 Ma. The basaltic andesites, which have a predominantly mantle-derived geochemical signature are thought to result from the mixing of dacitic magmas with MORB-type liquids derived from the buried spreading ridge. Two groups are distinguished among the dacites: the low-Si group has the chemical characteristics of adakitic slab melts, with depleted heavy rare earth element (HREE) abundances suggesting the occurrence of residual garnet in their source. The high-Si group has less depleted HREE contents. The Sr, Nd, and O isotopic signatures of both groups are $\in$Sr = −14.9 to +0.8, $\in$Nd = +2.9 to +3.8, and δ^{18}O values = +6.4 to +6.9‰ respectively, consistent with mixed magma sources that include a MORB-type component and sediments. We propose that the high-Si dacites are derived from the hydrous melting of a mixture of MORB and sediments at high temperatures (800°–900°C) under low pressures (<0.8 GPa). The low-Si dacites originate from the melting of a similar source under higher pressures consistent with depths of 25–45 km. Two scenarios accounting for the near-trench position of these latter rocks are envisioned. The first invokes rapid tectonic erosion and changes in sedimentary wedge geometry. The second one postulates that parts of the slab are subducted rapidly to depths of 20–30 km right under the trench. *INDEX TERMS:* 3640 Mineralogy and Petrology: Igneous petrology; 8120 Tectonophysics: Dynamics of lithosphere and mantle—general; 9360 Information Related to Geographic Region: South America; *KEYWORDS:* slab melting, Chile trench, ridge subduction, forearc magmatism, geochemistry, calc-alkaline magmatism

Citation: Guivel, C., Y. Lagabrielle, J. Bourgois, H. Martin, N. Arnaud, S. Fourcade, J. Cotten, and R. C. Maury, Very shallow melting of oceanic crust during spreading ridge subduction: Origin of near-trench Quaternary volcanism at the Chile Triple Junction, *J. Geophys. Res.*, *108*(B7), 2345, doi:10.1029/2002JB002119, 2003.

1. Introduction

[2] The emplacement of subduction-related magmas in near-trench position cannot be easily accounted for by the commonly admitted models of magma genesis in arcs [*Arculus*, 1994] but could be a consequence of ridge subduction [*Dickinson and Snyder*, 1979; *DeLong et al.*, 1979; *Thorkelson*, 1996]. In the geological record, the occurrence of anomalous near-trench magmatic activity in forearc domains has often been related to ancient Ridge-Trench-Trench triple junctions, e.g., in Japan [*Marshak and Karig*, 1977; *Kiminami et al.*, 1994; *Osozawa and Yoshida*, 1997], the Alaska margin [*Hibbard and Karig*, 1990; *Haeussler et al.*, 1995; *Harris et al.*, 1996; *Lytwyn et al.*, 1997, 2000], California [*Sharma et al.*, 1991; *Cole and Basu*, 1992, 1995], and Baja California [*Rogers et al.*, 1985; *Aguillón-Robles et al.*, 2001; *Benoit et al.*, 2002]. The corresponding magmatic products, usually exposed in ancient accretionary wedges, are predominantly bimodal. They include: (1) basaltic rocks transitional between normal Mid-Ocean-Ridge Basalts (MORB) and calc-alkaline basalts, which are thought to derive from the suboceanic mantle of the spreading ridge variously contaminated by subduction-related material either in front of the trench [*Klein and Karsten*, 1995; *Sturm et al.*, 1999; *Osozawa and Yoshida*, 1997; *Lytwyn et al.*, 1997], or during their ascent through the continental crust and accretionary prism [*Maeda and Kagami*, 1996]; and (2) evolved calc-alkaline magmas (granitic plutons or dacites and rhyolites) likely

[1]Laboratoire de Planétologie et Géodynamique, Université de Nantes, Nantes, France.
[2]Domaines Océaniques, Institut Universitaire Européen de la Mer, Université de Bretagne Occidentale, Plouzané, France.
[3]Institut de Recherche et Développement and Centre National de la Recherche Scientifique, Université Pierre et Marie Curie, Paris, France.
[4]Magmas et Volcans, Université Blaise Pascal, Clermont-Ferrand, France.
[5]Géosciences Rennes, Université de Rennes I, Rennes, France.

0148-0227/03/2002JB002119$09.00

derived from either anatexis of continental materials [*Johnson and O'Neil*, 1984; *Barker et al.*, 1992], anatexis of oceanic crust [*Harris et al.*, 1996], or interaction of ascending MORB magma with the accretionary prism [*Sharma et al.*, 1991; *Cole and Basu*, 1995; *Lytwyn et al.*, 2000].

[3] In this paper, we provide new geochemical and chronological data demonstrating that very recent, near-trench calc-alkaline magmatism is exposed in its initial tectonic position in the active Chile Triple Junction (CTJ hereafter) area (46°09′S) (Figure 1). In this area where the Chile Ridge is being subducted beneath the South America Plate, extremely fresh, Pleistocene calc-alkaline basaltic andesites and dacites have been dredged in the immediate vicinity of the CTJ during the CTJ cruise of R/V *L'Atalante* in 1997. These rocks, although geochemically rather similar to the Chilean arc lavas located 200 km landward, were sampled along the lower slope of the continental margin, less than 20 km landward from the trench axis [*Bourgois et al.*, 2000]. They are exposed above an oceanic slab less than 10 km deep, in a highly uncommon location for subduction-related magmas. The aim of the present study is to show that they mostly derive from very shallow hydrous melting of subducting oceanic basalts and associated sediments under high thermal conditions.

2. Geological Setting and Samples Studied

2.1. Triple Junction Motions

[4] Since at least 6 Ma, the Chile Ridge entering the trench consists of short segments separated by fracture zones. Segment 1 of the southern Chile Ridge entered the trench ca. 0.3 Ma (Figure 2). Previously, two short ridge segments were subducted after 6 and 3 Ma, west of the Taitao Peninsula, between the Esmeralda and the Tres Montes Fracture Zones, and between the Tres Montes and the Taitao Fracture Zones, respectively [*Leslie*, 1986; *Cande and Leslie*, 1986; *Tebbens et al.*, 1997]. Due to the N160 trend of the Chile Ridge (Figure 2), the Triple Junction migrated northward during subduction of spreading segments and slightly southward during subduction of fracture zones [*Cande and Leslie*, 1986]. Therefore the successive subduction of short segments separated by fracture zones led to the stagnation or back and forth motion of the Triple Junction along a restricted area of the margin where the studied lavas were dredged. Such a process is likely to produce a high thermal regime (the "blowtorch effect" of *DeLong et al.* [1979]). According to *Lagabrielle et al.* [2000], temperatures of 800°–900°C were attained at depths of 10–20 km below the CTJ area.

[5] The complex segment of the Chile margin between 45°50′S and 47°10′S, referred to as the synsubduction segment by *Bourgois et al.* [2000], is the locus of recent magmatic activity. It includes the Chile spreading ridge segment located between the Darwin and the Taitao fracture zones and currently subducting beneath the continental margin, the North Taitao Canyon and the Taitao Ridge bounded to the north by the North Taitao Ridge Fault (Figure 1). This fault offsets the subduction front right laterally. To the north of the North Taitao Ridge Fault, subduction-erosion removed most of the previously accumulated accretionary prism, which is preserved to the south along the Taitao Ridge.

2.2. Magmatic Samples From the CTJ Cruise

[6] Basaltic to dacitic lavas were collected during the CTJ cruise on both oceanic and continental sides of the Chile Trench. Dredge station locations are presented in Figure 1 and Table 1. Basaltic samples with pillow lava morphology were recovered along the western wall of the axial valley (dredge CTJ29) of the Southern Chile Ridge segment 1. Landward from the trench, dredges CTJ19, from the northern flank of the North Taitao Canyon, and CTJ16, located on the Taitao Ridge, near Site 862 of the Leg ODP 141, recovered greenschist facies dolerites and altered basalts, respectively. Very fresh basaltic andesites were sampled at two different sites: on a small volcanic edifice located on the continental edge of the trench close to the CTJ (CTJ28), and on the middle southwest slope of the Taitao Ridge (CTJ11). In addition, silicic lavas located only 8 km landward from the trench axis were recovered along the southern slope of the North Taitao Canyon (CTJ17). In this paper, we present geochemical data (major and trace elements, Sr-Nd and O isotopic compositions) obtained on these forearc, subduction-related volcanic rocks together with geochronological data confirming their recent to very recent ages of emplacement. New and previously published geochemical data from basalts of the Chile Ridge spreading segment 1 are also presented for comparison.

2.3. Analytical Procedures

[7] Twenty-one volcanic rocks ranging from basalts to dacites and one sediment from the Taitao Ridge were analyzed for the present study. They include 3 basalts from the CTJ29 dredge, 5 basaltic andesites from CTJ28 dredge, 2 basaltic andesites from CTJ11 dredge, and 11 dacites from CTJ17 dredge. Analyses were performed on handpicked chips of glass for dredged samples CTJ29, CTJ28, and CTJ11.

[8] Whole rock major and trace element analyses (Table 2) were obtained at Brest by inductively coupled plasma-atomic emission spectrometry (ICP-AES), except Rb which was measured by atomic absorption spectroscopy. Calibrations were made using standards PM-S, WS-E, BE-N, AC-E, JB-2, and SY-4 (see *Cotten et al.* [1995] for the analytical procedures). Relative standard deviations for major elements are <2% except for MnO and P_2O_5. Those for trace elements are <5%.

[9] Mineral analyses were obtained with a Cameca SX50 electron microprobe at Brest. Analytical conditions are described by *Defant et al.* [1991]. Representative mineral analyses are available as electronic supporting material[1].

[10] Sr and Nd isotopic compositions were determined by mass spectrometry at Clermont-Ferrand (analytical methods are described by *Pin and Paquette* [1997]). $^{87}Sr/^{86}Sr$ ratios were normalized to $^{86}Sr/^{88}Sr = 0.1194$ [*Faure*, 1986], and $^{143}Nd/^{144}Nd$ ratios were normalized to $^{146}Nd/^{144}Nd = 0.7219$. No age correction was applied to the measured Sr- and Nd-isotopic ratios presented in Table 3.

[11] Oxygen isotopic compositions were obtained on both whole rocks and separated pyroxenes in Rennes. Pyroxenes

[1] Auxiliary material for this article contains a data set (.txt) of representative mineral microprobe analyses obtained at Brest, France, on the CTJ lava population. Additional file information is provided in the README.txt. It can be found at ftp://ftp.agu.org/apend/jb/2002JB002119/2002JB002119-README.txt.

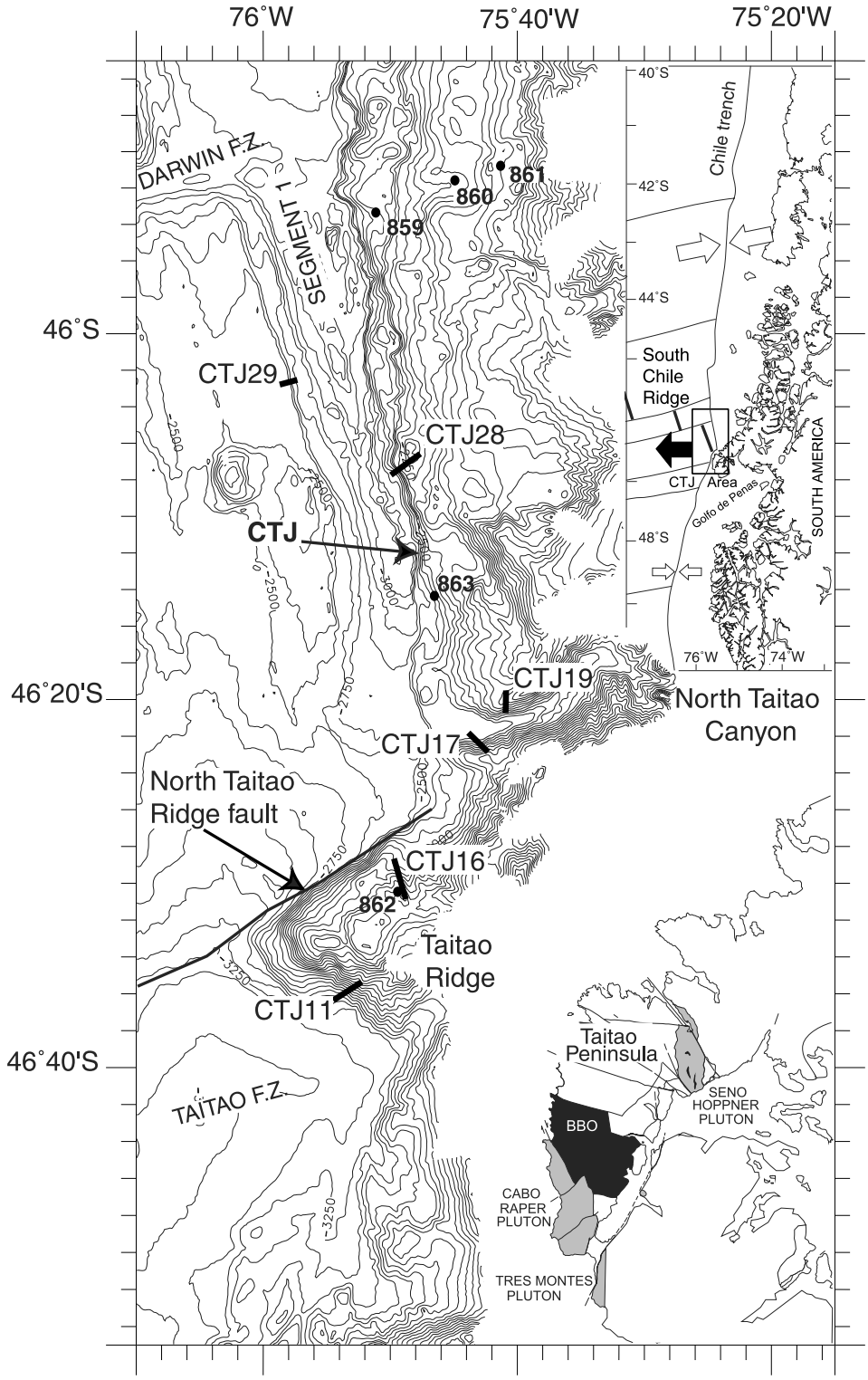

Figure 1. Bathymetric map (depths in m) of the synsubduction segment of the Chile margin as defined by *Bourgois et al.* [2000]. Location map is shown in the inset. Numbers 859–863 refer to Sites drilled during ODP Leg 141 [*Behrmann et al.*, 1994]. Lines refer to dredges hauls of the CTJ cruise that recovered magmatic material. These dredge sites allowed sampling of the three main morphotectonic units of the region, from north to south: (1) the segment 1 of the Chile spreading ridge entering the Chile Trench and limited by Darwin and Taitao Fracture Zones, (2) the North Taitao Canyon, and (3) the Taitao Ridge. Basalts were recovered at dredge-sites CTJ29, CTJ19, and CTJ16. Fresh basaltic andesites were recovered at dredge-sites CTJ28 and CTJ11. Dacites are localized at dredge-site CTJ17, along the southern wall of the North Taitao Canyon. CTJ, Chile Triple Junction; BBO, Bahia Barrientos Ophiolite. Inset, regional map with location of the study area; GP, Golfo de Penas.

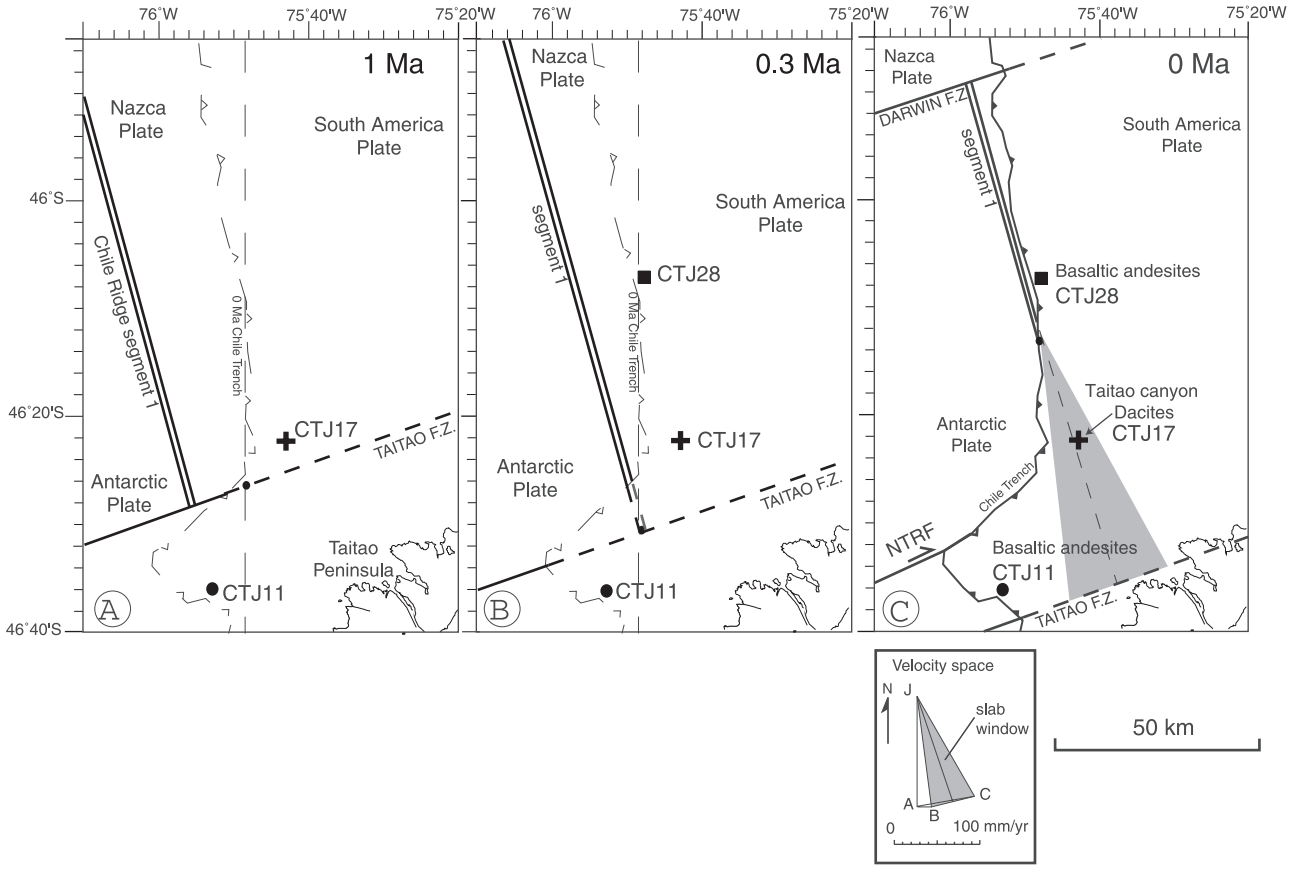

Figure 2. Chile Triple Junction (CTJ) plate configuration at: (a) 1 Ma, (b) 0.3 Ma, and (c) present-day setting with slab window formation during the last 0.3 Myr. Geometric construction is after *Thorkelson* [1996]. Rate of northward migration of the CTJ in Ridge-Trench-Trench configuration is 160 mm/yr. Rate of southward migration in Transform-Trench-Trench configuration is 10 mm/yr [*Cande and Leslie*, 1986]. Relative plate motion between Antarctica and South America: 20 and 84 mm/yr between Nazca and South America [*DeMets et al.*, 1990]. Half spreading rate of the Chile Ridge: 31.4 mm/yr [*Tebbens et al.*, 1997]. NRTF, North Taitao Ridge Fault. Basaltic andesites dredge sites CTJ28 and CTJ11 and dacites dredge site CTJ17 are localized.

were separated by classical rock crushing and heavy liquid techniques. Final sampling was hand done under binocular microscope. Oxygen was extracted from the pyroxenes using the BrF_5 method [*Clayton and Mayeda*, 1963] then converted to CO_2 and analyzed using a VG® SIRA*10* triple collector instrument (see *Fourcade et al.* [1994] for further information on the procedures). Results are expressed in Table 3 as ‰ $\delta^{18}O$ units relative to the V-SMOW standard reference.

[12] $^{40}Ar/^{39}Ar$ radiometric ages presented in Table 4 were measured in Clermont-Ferrand. Whole rocks were crushed, sieved, and individual grains chosen under binocular microscope. All separates were irradiated in a single irradiation experiment at the Ford reactor of the University of Michigan for a total fluence of 10^{18} n/cm^2. *J* factor was estimated by the use of duplicates of the Fish Canyon sanidine standard with an age of 27.55 ± 0.08 [*Lanphere and Baadsgaard*, 2001] at a value of 0.01028 with 1% relative standard deviation. Interfering nuclear reactions on K and Ca were calculated by coirradiation of pure salts, but K/Ca and Cl/K plots are given for comparison with the age spectra and are only qualitative as they represent $^{39}Ar/^{37}Ar$ and $^{38}Ar/^{39}Ar$

Table 1. Dredge Station Locations for R/V *L'Atalante* CTJ Cruise (1997)

			On-Bottom			Off-Bottom		
Station	Structure/Unit	Nature	Latitude, °S	Longitude, °W	Depth, m	Latitude, °S	Longitude, °W	Depth, m
CTJ29	SCR1 segment	basalts	46°02.64′	75°57.12′	2868	46°02.93′	75°58.72′	2562
CTJ28	internal wall margin	basaltic andesites	46°07.82′	75°49.86′	2830	46°06.70′	75°47.52′	2194
CTJ43	Taitao Canyon	dacites	46°19.53′	75°35.97′	2178	46°18.77′	75°36.68′	1626
CTJ19	Taitao Canyon	basalts	46°20.80′	75°40.80′	2362	46°19.5′	75°41.0′	1852
CTJ17	Taitao Canyon	dacites	46°22.20′	75°43.40′	2570	46°22.95′	75°42.32′	1689
CTJ16	Taitao Ridge	basalts	46°28.70′	75°49.50′	1880	46°31.0′	75°48.9′	1240
CTJ11	Taitao Ridge	basaltic andesites	46°36.22′	75°54.41′	3100	46°35.43′	75°52.20′	2126

Table 2. Whole Rock Analyses of Chile Triple Junction Lavas Ranging From Basalts to Dacites and CTJ11-10(s) Sediment From the Taitao Ridge Used in the Partial Melting Modeling[a]

	DL	CTJ29-1[b]	CTJ29-3[b]	CTJ29-4[b]	CTJ28-1[b]	CTJ28-2[b]	CTJ28-4[b]	CTJ28-5[b]	CTJ28-8[b]	CTJ11-5[b]	CTJ11-6[b]	CTJ11-10(s)	CTJ17-28	CTJ17-5	CTJ17-2	CTJ17-20	CTJ17-25	CTJ17-15	CTJ17-8	CTJ17-12	CTJ17-21	CTJ17-22	CTJ17-7
Unit		SCR1	SCR1	SCR1	OAV	OAV	OAV	OAV	OAV	TR	TR	TR	TC	TC	TC	TC	TC	TC	TC	TC	TC	TC	TC
Nature		B	B	B	BA	BA	BA	BA	BA	BA	BA	S	LSD	LSD	HSD	HSD	HSD	HSD	HSD	HSD	HSD	HSD	HSD
SiO_2, wt %		50.45	50.30	50.5	53.65	53.35	53.4	53.6	53.6	57.35	57.5	60.80	65.50	65.70	68.50	68.40	69.50	68.80	68.65	68.60	68.9	69.3	68.10
TiO_2, wt %		1.6	1.55	1.54	0.94	0.92	0.94	0.93	0.91	0.8	0.8	0.81	0.42	0.45	0.46	0.44	0.44	0.45	0.51	0.49	0.44	0.45	0.55
Al_2O_3, wt %		15.52	15.30	15.18	17.5	17.3	17.35	17.35	17.1	16.4	16.6	15.05	16.45	16.42	15.70	15.75	15.15	15.10	15.25	14.65	15.05	15.1	16.10
Fe_2O_3, wt %[c]		10.7	10.45	10.38	6.97	6.98	7.05	6.96	6.78	5.47	5.42	6.20	3.00	3.14	2.97	2.88	2.73	2.96	3.18	2.81	2.78	2.87	3.02
MnO, wt %		0.18	0.17	0.17	0.12	0.12	0.13	0.13	0.12	0.09	0.09	0.08	0.06	0.06	0.05	0.05	0.05	0.05	0.05	0.05	0.05	0.05	0.05
MgO, wt %		7.76	7.54	7.52	6.3	6.45	6.48	6.35	6	5.86	5.55	3.31	1.90	1.92	1.60	1.54	1.49	1.73	1.48	1.04	1.63	1.7	1.21
CaO, wt %		11.25	10.96	11.08	9.45	9.3	9.4	9.45	9.3	8	7.85	3.77	4.82	4.79	3.93	3.92	3.47	3.61	3.65	2.97	3.6	3.45	3.46
Na_2O, wt %		2.83	2.79	2.76	3.25	3.21	3.2	3.22	3.15	3.43	3.59	3.41	3.95	3.95	4.25	4.08	4.21	4.11	4.23	4.14	4.1	4.2	4.69
K_2O, wt %		0.16	0.16	0.16	0.68	0.68	0.67	0.67	0.65	1.05	1.1	1.74	1.30	1.50	1.89	1.90	2.12	2.12	2.29	2.62	1.97	2.03	2.66
P_2O_5, wt %		0.17	0.16	0.17	0.21	0.22	0.21	0.21	0.21	0.12	0.13	0.21	0.12	0.14	0.10	0.10	0.10	0.10	0.12	0.10	0.1	0.1	0.12
LOI		**−0.7**	**−0.03**	**0.18**	**1.13**	**1.18**	**1.12**	**1.31**	**1.81**	**1.74**	**1.54**	**4.19**	**1.74**	**2.02**	**0.71**	**0.88**	**0.33**	**0.71**	**0.66**	**2.46**	**0.69**	**0.99**	**0.18**
Sum		**99.92**	**99.35**	**99.64**	**100.2**	**99.71**	**99.95**	**100.18**	**99.63**	**100.31**	**100.17**	**99.57**	**99.26**	**100.09**	**100.16**	**99.94**	**99.59**	**99.74**	**100.07**	**99.93**	**99.31**	**100.24**	**100.14**
Rb, ppm	1	3.6	4	3.4	20.5	21.5	20	19.8	19.6	42.5	43	53	37.5	44	84	39	78.5	45.5	86	107	49.5	38.5	107
Sr, ppm	1	128	128	127	205	200	203	203	202	177	177	290	465	430	246	250	183	186	177	146	186	183	178
Ba, ppm	3	34	33	35	125	128	125	125	130	205	208	340	348	346	398	400	422	417	612	438	412	420	465
Sc, ppm	0.2	37.5	36	37	23	23	23	22.8	23	18.3	18.6	17.5	6.3	6.5	7.4	6.7	6.3	7	7.2	6.5	6.7	6.6	7.3
V, ppm	3	278	295	300	155	154	152	150	152	125	126	138	47	45	50	46	44	48	50	49	41	46	56
Cr, ppm	2	277	281	295	155	175	160	170	170	140	127	61	22	22	22	21	28	33	22	11	31	31	14
Co, ppm	2	42	39	40	25	28	27	27	25	22	22	15	9	9	8	7	7	8	8	6	7	7	7
Ni, ppm	2	115	126	110	85	101	95	86	80	107	95	25	29	28	16	15	28	33	20	9	32	32	11
Y, ppm	0.5	36	36	34	24.3	25.5	25	24.7	26.8	20.8	21	24	12.2	13.4	17	17.9	19.8	20	23.5	24.5	20.7	20.5	25.5
Zr, ppm	2	114	112	116	160	155	158	155	162	128	131	75	153	153	148	140	130	122	155	101	128	119	118
Nb, ppm	1	4.2	3.7	3.8	8.2	8.4	8.1	8	7.8	7.9	7.7	8.7	3.9	4.6	5.3	5.4	6.3	6.4	7.5	7.7	6.1	5.9	7.9
La, ppm	1	4.8	4.7	4.7	12.2	12.2	12.4	12.2	12.5	12.3	12.5	20.7	13.8	13.8	16.6	16.8	18.4	18.5	19.2	21	18	18.3	21.4
Ce, ppm	2	14	13	13	27.5	25.5	27.4	26.5	28	24	25	44	28	30.5	34	33.5	36	36.5	39.5	40.5	36	36	42
Nd, ppm	2	12	12	11.5	14.6	15.2	14.8	14.5	14	12.5	12.6	21.5	12	14.6	16.5	15	16	16.5	18.2	19.2	15.4	16.4	20.5
Sm, ppm	0.6	3.8	4	3.8	3.5	3.45	3.7	3.4	3.8	3	3	5	2.7	2.7	3.15	3.3	2.9	3.3	3.6	4	3.4	3.4	4.35
Eu, ppm	0.2	1.32	1.35	1.32	1.14	1.09	1.12	1.09	1.15	0.89	0.93	1.2	0.72	0.75	0.8	0.78	0.82	0.79	0.87	0.83	0.82	0.78	0.92
Gd, ppm	0.6	5.5	5.2	4.9	4.1	4.1	4.3	4.2	3.7	3.4	3.4	4.1	1.9	2.55	3.15	2.8	2.9	3.3	3.8	4	3.1	3.2	4.3
Dy, ppm	0.4	6.2	5.95	5.85	4.3	4.25	4.35	4.2	4.15	3.4	3.5	4.25	1.85	2.15	2.9	2.8	3.05	3.25	3.5	3.95	3.05	3.2	4.15
Er, ppm	1	3.7	3.7	3.6	2.45	2.6	2.5	2.5	2.5	2.1	2.1	2.15	1.15	1.35	1.7	1.65	2	2	2.2	2.4	2	1.9	2.55
Yb, ppm	0.2	3.67	3.62	3.45	2.55	2.46	2.54	2.52	2.57	2.08	2.12	2.23	1.15	1.31	1.7	1.7	1.94	1.98	2.05	2.4	1.95	1.98	2.48
Th, ppm	0.1	0.4	0.5	0.45	2.9	2.9	2.5	2.8	2.7	5	5.1	6.2	3.7	4.7	7.2	7.65	8.5	8.3	9.3	10.8	8.1	8.4	10.5

[a]SCR1, Southern Chile Ridge segment 1; DL, detection limit; OAV, off-axis volcano; TR, Taitao Ridge; TC, Taitao Canyon; B, basalt; BA, basaltic andesite; S, sediment; LSD, low-Si dacite; HSD, high-Si dacite; LOI, loss on ignition.

[b]Analyses were performed on separated chips of glass.

[c]Total Fe as Fe_2O_3.

Table 3. Isotopic and Chemical Data for Chile Triple Junction Rocks: Selected Southern Chile Ridge Basalts From Segment 1 (CTJ29), Basaltic Andesites From Volcano Located on the Edge of the Trench (CTJ28) and From Taitao Ridge (CTJ11), Selected Taitao Canyon Dacites From Dredge CTJ17; CTJ11-10(s) Sediment Used in the Partial Melting Modeling[a]

	$\delta^{18}O$, ‰ versus V-SMOW	$^{87}Sr/^{86}Sr$	$\in Sr$	$^{143}Nd/^{144}Nd$	$\in Nd$	SiO_2, wt %	LOI, wt %
			Basalts				
CTJ29-3 Gl	+5.77 ± 0.05	0.702734 ± 7	−25.1	0.513117 ± 4	+9.3	50.3	−0.03
CTJ29-4 Gl	+5.70 ± 0.05	0.702804 ± 6	−24.1	0.513118 ± 4	+9.4	50.5	0.18
			Basaltic Andesites				
CTJ28-1 Gl	+5.92 ± 0.12	0.703684 ± 17	−11.6	0.512905 ± 10	+5.2	53.65	1.13
CTJ28-4 Gl	+6.04 ± 0.10	0.703688 ± 12	−11.5	0.51292 ± 10	+5.5	53.4	0.21
CTJ28-5 Gl	+6.35 ± 0.02	0.703679 ± 13	−11.6	0.512921 ± 10	+5.5	53.6	1.31
CTJ28-8 Gl	+6.10 ± 0.06	0.703707 ± 6	−11.3	0.512932 ± 4	+5.7	53.6	1.81
CTJ11-5 Gl	+6.51 ± 0.04	0.703663 ± 12	−11.9	0.512876 ± 9	+4.6	57.35	1.74
CTJ11-6 Gl	+6.40 ± 0.02	0.703662 ± 14	−11.9	0.512868 ± 8	+4.5	57.5	1.54
			Sediment				
CTJ11-10(s)	+10.48	0.706371 ± 7	+26.6	0.512533 ± 6	−2.0	60.8	4.19
			Dacites				
CTJ17-7 WR	+7.23 ± 0.11	0.704555 ± 6	+0.8	0.512817 ± 6	+3.5	68.1	0.18
Px	+6.63						
Magma	+6.9						
CTJ17-12 WR	no data	0.704485 ± 7	−0.2	0.512832 ± 5	+3.8	68.6	2.46
Px	+6.22						
Magma	+6.5						
CTJ17-20 WR	+7.96	0.704436 ± 6	−0.9	0.512801 ± 5	+3.2	68.4	0.88
Px	+6.1						
Magma	+6.4						
CTJ17-21 WR	no data	0.704164 ± 13	−4.8	0.512788 ± 10	+2.9	68.9	0.69
CTJ17-5 WR	no data	0.703453 ± 14	−14.9	0.512818	+3.5	65.7	2.02
CTJ17-28 WR	no data	0.704216 ± 16	−4.0	0.512808 ± 20	+3.3	65.5	1.74

[a]WR, whole rocks; Px, separated pyroxenes; and magma, $\delta^{18}O$-magmatic values obtained from $\delta^{18}O$-values of pyroxenes +0.3‰ [*Sheppard and Harris*, 1985]. Uncertainties quoted correspond to duplicate O extractions. $^{87}Sr/^{86}Sr$ ratios were normalized to $^{86}Sr/^{88}Sr = 0.1194$ [*Faure*, 1986], and $^{143}Nd/^{144}Nd$ ratios were normalized to $^{146}Nd/^{144}Nd = 0.7219$. Values of $\in Sr$ are calculated relative to a present-day uniform reservoir of $(^{87}Sr/^{86}Sr)_{today} = 0.7045$ [*DePaolo*, 1988] and $\in Nd$ values are calculated relative to a chondritic uniform reservoir (CHUR) of $(^{143}Nd/^{144}Nd)_{today} = 0.512638$. Replicate standard analyses average 0.710261 ($\sigma = 1.03 \times 10^{-5}$, $n = 3$) for $^{87}Sr/^{86}Sr$ for NBS-987 and 0.511951 ($\sigma = 3.2 \times 10^{-6}$, $n = 3$) for $^{143}Nd/^{144}Nd$ for Ames standard.

used as proxies for the true elemental ratios. Samples were loaded in aluminum packets into a frequency furnace, the temperature of which is calibrated by means of an optical pyrometer, and step heated in a classical fashion from usually 700° to 1400°C. Each step lasted for 20 min. The gas was purified by means of cold traps with liquid air and Al-Zr getters. Once cleaned, the gas was introduced into a VG3600 mass spectrometer, and 2 min was allowed for equilibration before analysis was done statistically. Signals were measured by means of a Faraday cup with a resistor of 10^{11} ohm for ^{40}Ar and ^{39}Ar while ^{39}Ar, ^{38}Ar, ^{37}Ar, and ^{36}Ar were analyzed with a photomultiplier after interaction on a Daly plate. Gain between both collectors was estimated by duplicate analysis of ^{39}Ar on both during each analysis and also by statistical analysis over a period of several years. The gain is (on average) 95 and is known to better than 1.5%. This error is included in the age calculation, along with analytical errors on each signal and errors on the blank values. Detailed analytical results are available from the authors upon request. Only age spectra and isochron results will be presented therein. When age plateau are given they are weighted mean plateaus [*Dalrymple and Lanphere*, 1974], which takes the error on the *J* factor into account.

2.4. Analytical Results

2.4.1. Petrography and Mineralogy

2.4.1.1. Basalts

[13] The basalts CTJ29 from the Southern Chile Ridge segment 1 are vesicular pillow lava fragments with glassy rims. Their groundmass texture is spherulitic and they contain less than 10 modal% euhedral plagioclase phenocrysts (An_{87-82}) together with olivine (Fo_{86-83}) (Figure 3a) and less calcic plagioclase (An_{63-60}) microcrysts.

2.4.1.2. Basaltic Andesites

[14] The basaltic andesites from dredge CTJ28 are very fresh vesicular pillow lava fragments with a 2-mm-thick glassy margin. They are olivine-(Fo_{87-84}) and plagioclase (An_{86-81}) bearing slightly porphyritic lavas. Their groundmass contains plagioclase (An_{74}) microlites, chromite, and subordinate clinopyroxene (Figure 3b). The Taitao Ridge basaltic andesites from dredge CTJ11 have pillow lava morphologies with glass crusts. They are vesicular, olivine-phyric lavas with plagioclase (An_{70-55}) laths and augite microphenocrysts (Figure 3b) in the groundmass.

Table 4. $^{40}Ar/^{39}Ar$ Ages Data[a]

Sample	$^{40}Ar/^{39}Ar$ Ages, Ma	Mineral/Glass
	Basaltic Andesites	
CTJ28-2	<0.127	glass
CTJ28-4	<0.070	glass
CTJ11-5	<2	glass
CTJ11-6	1.14 ± 0.11	glass
	Dacites	
CTJ17-21	<1.12	amphibole
CTJ17-22	<0.280	amphibole

[a]See text for further information.

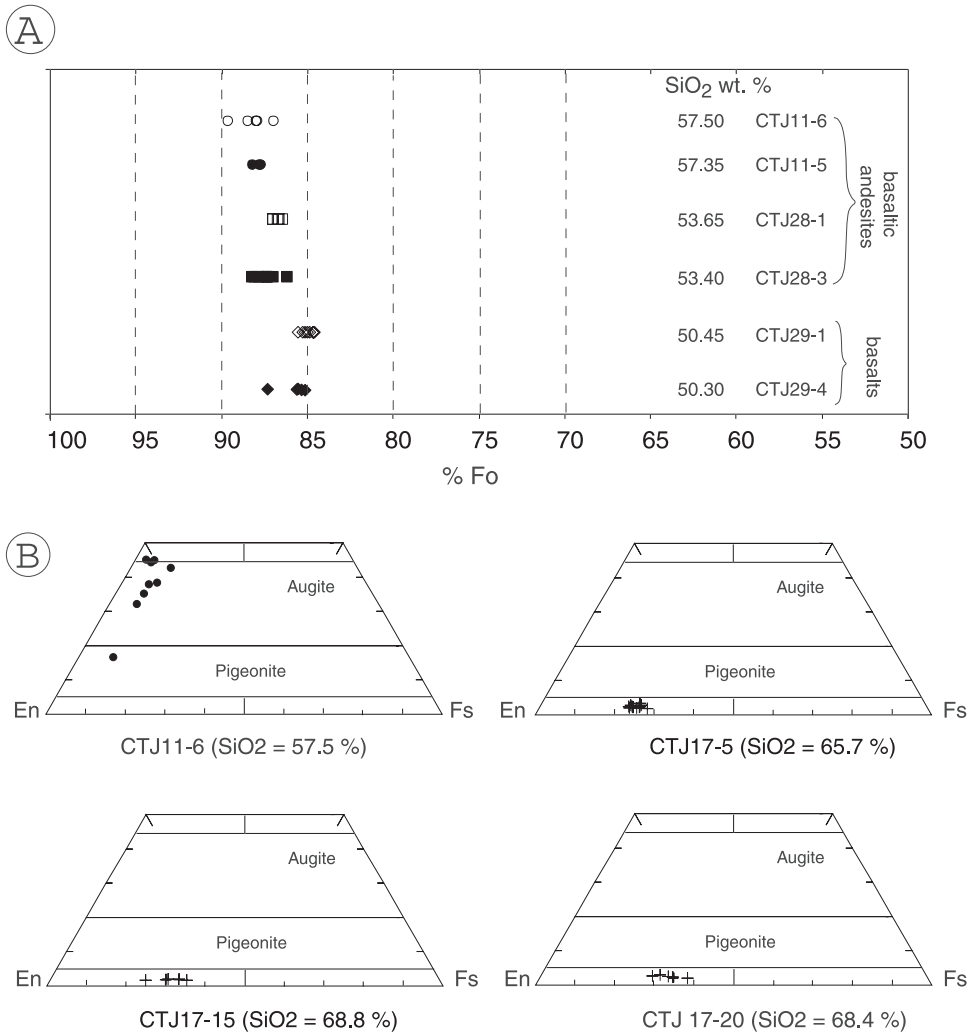

Figure 3. (a) Fo composition of analyzed olivines; (b) Wo-En-Fs identification diagram for analyzed pyroxenes (terminology from *Morimoto et al.* [1988]).

Olivine phenocrysts have homogeneous compositions (Fo_{89-86}), which are significantly richer in Mg than olivine phenocrysts within basalts (Figure 3a). Several dredged samples contain fragments of young sediments adjacent to the basaltic andesites. These sediments contain glass shards, a feature which suggests that their deposition was concomitant with the emplacement of the basaltic andesites. One of these sediments (CTJ11-10s) has been selected for geochemical analysis.

2.4.1.3. Dacites

[15] The CTJ dacites are fresh, plagioclase-phyric lavas with subordinate orthopyroxene in cluster with the plagioclase (An_{66-42}) phenocrysts. Two dacitic samples (CTJ17-5 and CTJ17-28) are dark grey, vesicular lavas, the only phenocrysts of which are plagioclase and orthopyroxene. All the others are light grey plagioclase- and orthopyroxene-bearing dacites which, in addition, contain variable amounts of Fe-Ti oxides, brown amphibole, and rare clinopyroxene phenocrysts. Groundmass textures vary from trachytic to hyalopilitic. Orthopyroxene which is the dominant mafic phenocryst is always hypersthene (Figure 3b). Orthopyroxene phenocrysts from samples CTJ17-5 and CTJ17-28 have more primitive compositions (Mg-number [100(Mg/(Mg + Fe^{2+})] at ~75) than hypersthene from the light grey dacites. In the latter, the Mg-numbers vary from ca. 69 in dacite CTJ17-15 to 65 in CTJ17-2 dacite.

2.4.2. Major Element Data

[16] The CTJ volcanic rocks range in SiO_2 from 50.3 to 69.5 wt %. Basaltic to intermediate lavas, ranging in composition from 50.3 to 57.5 SiO_2 wt %, coexist with felsic lavas displaying a more restricted SiO_2 range (from 65.5 to 69.5 wt %). The lack of compositions between 58 and 65 SiO_2 wt % highlights the bimodal character of these subduction ridge-related lavas. K_2O wt % and FeO*/MgO (assuming FeO* = 0.9 $Fe_2O_3^*$) versus SiO_2 wt % variation diagrams are presented in Figure 4. All lavas, except basalts from the Southern Chile Ridge segment 1 (CTJ29) fall within the calc-alkaline fields defined by *Le Maître et al.* [1989] (Figure 4a) and *Miyashiro* [1974] (Figure 4b).

[17] Basalts from the inner wall of the Southern Chile Ridge segment 1 plot in Figure 4a diagrams as low-K (tholeiitic) lavas. Their major element compositions are within the range of common MORB and, in particular, they are close to the Normal-MORB (N-MORB) of the Southern

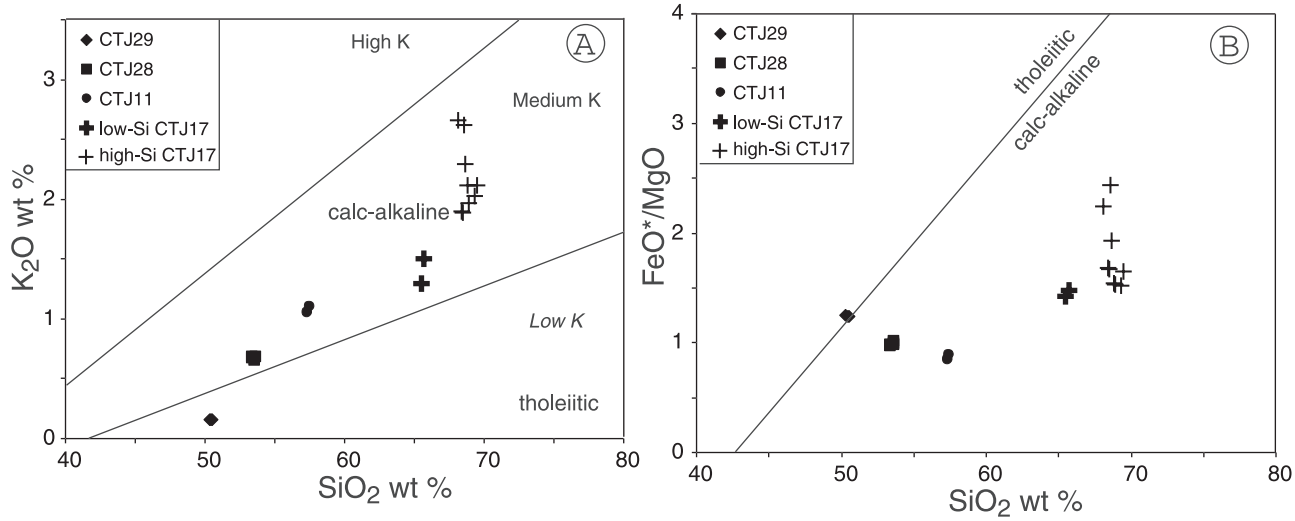

Figure 4. (a) K_2O versus SiO_2 classification diagram showing the Chile Triple Junction (CTJ) samples. The diagram shows the subdivisions of *Le Maître et al.* [1989]. (b) FeO*/MgO ratios (assuming FeO* = 0.9 $Fe_2O_3^*$) versus SiO_2 diagram showing the CTJ samples. Subdivision between tholeiitic and calc-alkaline magmas is after *Miyashiro* [1974].

Chile Ridge defined by *Sherman et al.* [1997a] on the basis of K/Ti < 0.15. The basaltic andesites from the volcanic edifice located on the edge of the trench (CTJ28), the Taitao Ridge basaltic andesites (CTJ11), and the North Taitao Canyon dacites (CTJ17) all plot within the medium-K calc-alkaline field (Figure 4a). Major elements either increase (Na_2O, K_2O) or decrease (Al_2O_3, CaO, MgO, $Fe_2O_3^*$, and TiO_2) regularly from basaltic andesites to dacites with increasing SiO_2 concentrations. All these lavas have low-TiO_2 contents (0.94–0.42 wt %) characteristic of calc-alkaline lavas. The basaltic andesites from CTJ28 show a limited range of SiO_2 contents (53.35–53.65 wt %) and are characterized by FeO*/MgO ranging from 0.97 to 1.02. The basaltic andesites from CTJ11 have higher SiO_2 contents (57.35 and 57.5 wt %) and lower FeO*/MgO (0.84–0.88) than those of the basaltic andesites from CTJ28 or of the CTJ17 dacites (1.42–2.43). The CTJ dacites range in SiO_2 from 65.5 to 69.5 wt %. Two groups of dacites, low-Si (65.5–65.7) and high-Si (68.1–69.5), can be distinguished, in accord with their petrographic features. The two dark grey samples (CTJ17-5 and CTJ17-28) belong to the low-Si group and have lower Na_2O and K_2O contents and concomitantly higher MgO, CaO, and Al_2O_3 contents. Their major element compositions are within the range of those of the adakites from the Austral Volcanic Zone [*Stern and Kilian*, 1996]. The major element features of the high-Si dacites are similar to those of the dacites from the South Volcanic Zone [*Gerlach et al.*, 1988], although the former are richer in Al_2O_3, MgO, and CaO and poorer in Fe_2O_3, TiO_2, Na_2O, and K_2O.

2.4.3. Trace Element Data

[18] Trace element abundance patterns normalized to the composition of N-MORB [*Sun and McDonough*, 1989] are shown in Figure 5. Representative basaltic samples D14-9 and D20-1 from the Chile Ridge segment 1 [*Klein and Karsten*, 1995] have been plotted in Figure 5a for comparison. Sample D14-9 represents a typical N-MORB showing depletion in large ion lithophile elements (LILE) and light rare earth elements (LREE). Sample D20-1 represents N-MORB magma with selective trace element enrichments (such as Rb, Ba, and K) or depletions (Nb relative to K and La) indicative of incorporation of a subduction-related component [*Klein and Karsten*, 1995]. The CTJ29 basalts are LREE-depleted (chondrite-normalized $(La/Sm)_N < 0.8$) as are samples D14-9 and D20-1. They are slightly enriched in LILE-like sample D20 but lack the significant depletions in Nb (relative to K and La) typical of subduction component.

[19] In the N-MORB-normalized plot, all of the basaltic andesites and dacites have LILE and LREE enrichments and Nb and Ti depletions relative to adjacent incompatible elements (Figures 5b and 5c, respectively). These features are characteristic of arc magmas. Chondrite-normalized $(La/Sm)_N$ increases with SiO_2 content from CTJ28 basaltic andesites to CTJ17 dacites [CTJ28, $(La/Sm)_N > 2.1$; CTJ11, $(La/Sm)_N > 2.6$; and CTJ17, $(La/Sm)_N$ ranging from 3.1 to 4].

[20] Low-Si dacites are characterized by moderately fractionated REE patterns, with $(La/Yb)_N$ of 7.5 and 8.5, slightly higher than those of high-Si dacites [$(La/Yb)_N$ ranging from 6.2 to 7.00]. The distinction between low-Si and high-Si dacites is especially based on Sr, Y, and heavy rare earth element (HREE) abundances. Low-Si dacites have higher Sr contents, lower Y and HREE concentrations, and lack a negative Eu anomaly. These features are typical of adakitic (slab-melt) compositions [*Defant and Drummond*, 1990]. Evolved lavas (SiO_2 > 63 wt %) from the Austral Volcanic Zone and from the Southern Volcanic Zone, respectively, have been plotted together with the North Taitao Canyon CTJ17 dacites in the Sr/Y versus Y diagram of Figure 6. The latter are intermediate between normal calc-alkaline, mantle-derived magmas (South Volcanic Zone magmas in Figure 6), and adakites/slab melts (Austral Volcanic Zone magmas in Figure 6).

2.4.4. Sr, Nd, and O Isotopic Compositions

[21] Sr, Nd, and O isotopic data for the CTJ lavas are given in Table 3, together with absolute errors, and plotted in Figure 7. The $^{87}Sr/^{86}Sr$ values of CTJ magmas range from

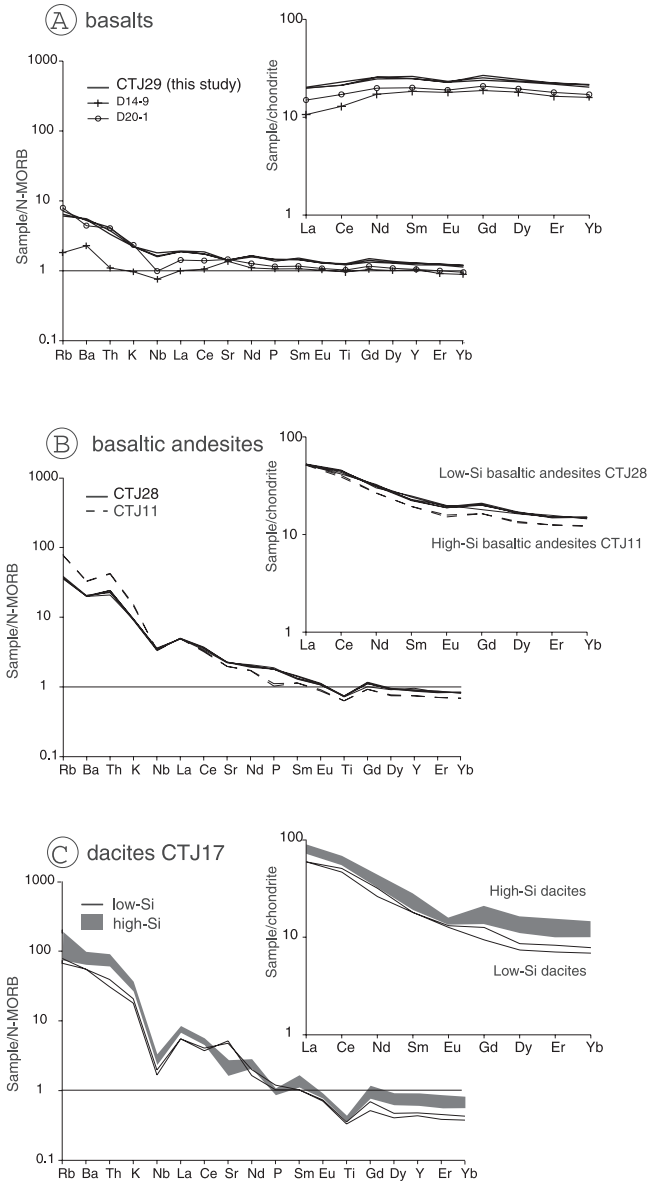

Figure 5. Trace element abundance patterns for representative Chile Triple Junction magmas normalized to the composition of N-MORB [*Sun and McDonough*, 1989]. The inset shows rare earth element patterns for the same samples normalized to chondritic values [*Sun and McDonough*, 1989]. (a) Basalts from Southern Chile Ridge segment 1 (CTJ29); D14-9 and D20-1 are representative basaltic samples from segment 1 [*Klein and Karsten*, 1995] shown for comparison; (b) basaltic andesites from dredges CTJ28 (continuous lines) and CTJ11 (dashed lines); and (c), Taitao Canyon dacites (CTJ17 dredge site); continuous lines, low-Si dacites; grey area, high-Si dacites; low-Si dacites are Y and HREE-depleted, and Sr enriched with no Eu negative anomaly. They share some chemical characteristics with adakitic magmas. High-Si dacites resemble normal calc-alkaline mantle-derived magmas.

0.70273 ± 1 for a basalt from the Chile Spreading Ridge segment 1 to 0.70455 ± 1 for one high-silica dacite (CTJ17-7) from the North Taitao Canyon. In the same samples, the $\in$Nd ranges from +9.3 to +3.5. The $\delta^{18}O$ varies from +5.8 measured for a basaltic glass to +6.9‰ in a dacite (the latter value deduced from $\delta^{18}O$ values measured on pyroxene).

[22] In order to discuss the origin of the isotopic data, we have also plotted in Figure 7a literature data from Chile Ridge basalts [*Klein and Karsten*, 1995], from South Volcanic Zone lavas [*Lopez-Escobar et al.*, 1993], and from the Austral Volcanic Zone adakites [*Stern and Kilian*, 1996]. The Sr and Nd isotopic compositions of the CTJ lavas fall within the range of the suboceanic Chile Ridge mantle, with slightly higher Sr isotope compositions for intermediate to felsic magmas (Figure 7a). The Chile Ridge mantle is highly heterogeneous and is interpreted as being variably contaminated by recycled oceanic crust and sediments [*Klein and Karsten*, 1995; *Sturm et al.*, 1999].

[23] Comparing the isotopic compositions of the dacites with those of the basaltic andesites recovered in the CTJ area, we observe a progressive enrichment in $^{87}Sr/^{86}Sr$ ratios correlated with depletion in the $^{143}Nd/^{144}Nd$ ratios from basalts to dacites. The $\delta^{18}O$ magmatic values of dacites are higher than typical MORB-type values (+5.7 ± 0.3‰) and also higher than those measured either on the Chile Ridge basalts [+5.6 to +6.0‰, *Sherman et al.*, 1997b] or on the CTJ basaltic andesites (+5.9 to +6.5‰, Figure 7b). Therefore the isotopic composition of the dacites indicates a contribution of crustal material. However, these dacites appear to have a lesser oxygen and/or strontium crustal imprint than some South Volcanic Zone lavas and the majority of Austral Volcanic Zone adakites erupted far away from the trench, across a 30-km-thick continental crust [*Stern and Kilian*, 1996].

2.4.5. $^{40}Ar/^{39}Ar$ Age Data

[24] Attempts to date the CTJ29 Chile Ridge basalts were unsuccessful because of their low-K contents. Among the

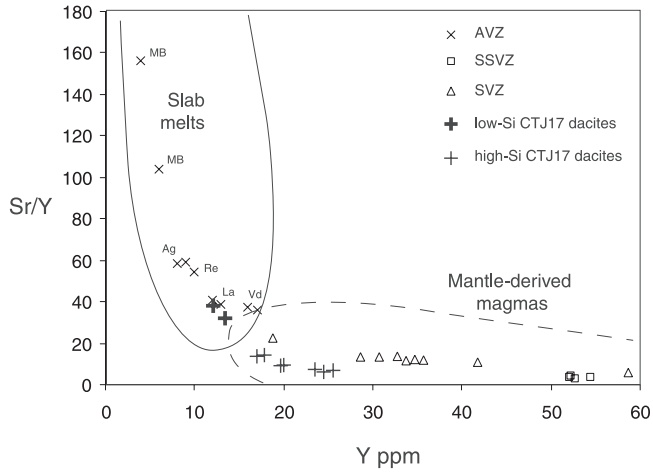

Figure 6. Sr/Y versus Y diagram showing fields expected for slab melts (solid curve) and mantle-derived magmas (dashed curve) [*Maury et al.*, 1996]. All CTJ17 dacites plot between the slab melt field and the mantle-derived field. The Austral Volcanic Zone lavas classified as adakites [*Stern and Kilian*, 1996] and the South Volcanic Zone [*Lopez-Escobar et al.*, 1993] lavas that include "normal" dacites from the Southern South Volcanic Zone [*Gerlach et al.*, 1988] are also shown for comparison. Austral Volcanic Zone volcanoes from south to north: MB, Mount Burney; Re, Reclus; Ag, Aguilera; Vd, Viedma; La, Lautaro.

higher SiO_2 lavas, sample CTJ11-6 yields a good plateau age at 1.14 ± 0.11 Ma, in agreement with the isochron age. In most cases, the low amount of K in the lavas coupled with young ages prohibits calculation of age plateaus, and in many instances, calculation returned null ages. To overcome that problem, maximum ages have been calculated using the blank values obtained at 500°, 1000°, and 1200°C prior to the analysis of the samples. Using that proxy, the following maximum ages were obtained (Table 4): 1.14 ± 0.11 Ma for basaltic andesite CTJ11-6, less than 1.12 Ma for CTJ17-21, and less than 0.28 Ma for CTJ17-22 high-Si dacites. CTJ28-2 and CTJ28-4 basaltic andesites, which have yielded $^{40}Ar/^{39}Ar$ glass ages lower than 127 and 70 ka, respectively, are likely to represent the youngest samples of our set.

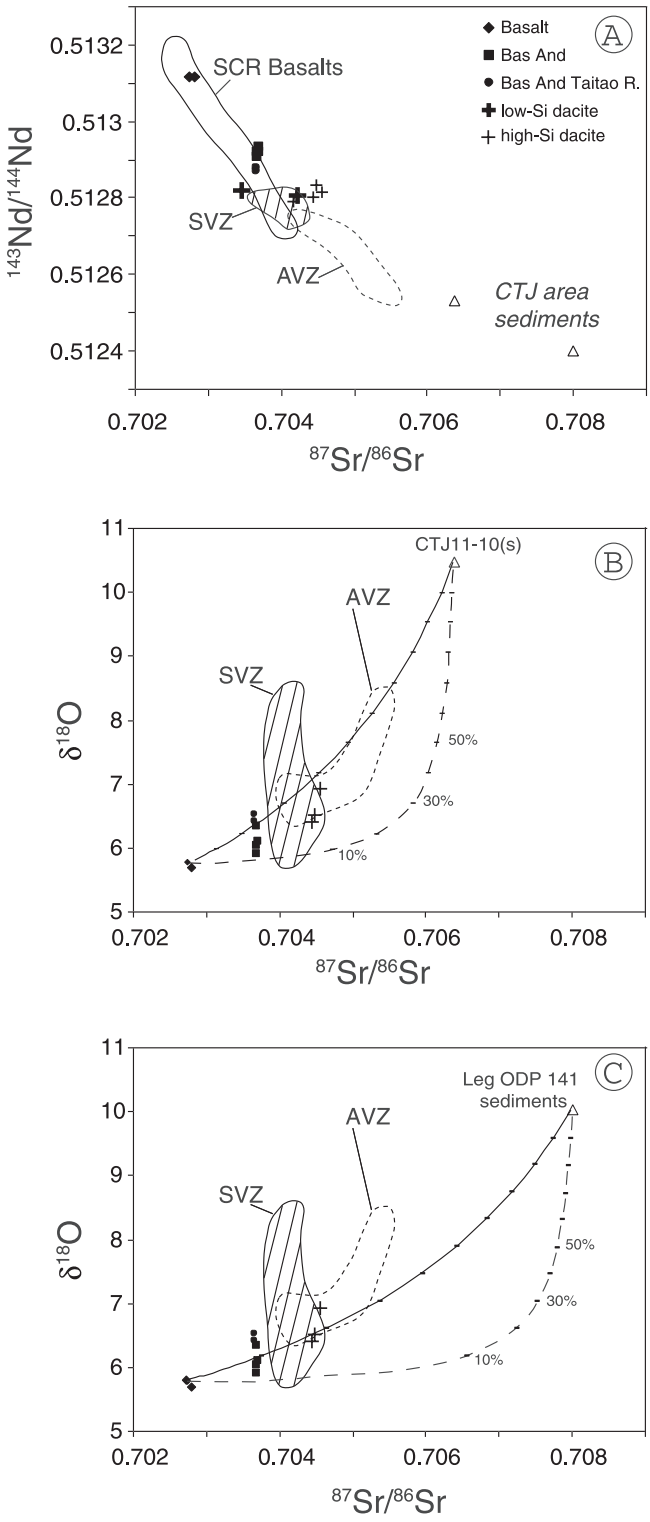

Figure 7. (opposite) Sr-Nd-O isotopic plots. (a) $^{143}Nd/^{144}Nd$ versus $^{87}Sr/^{86}Sr$ for CTJ lavas; (b and c) combined Sr and O isotopic plots. Curves on Figures 7b and 7c represent calculated mixing models for: solid curve, shallow-level contamination of N-MORB magma (CTJ29-3 Gl sample) by either sediments underlying the Taitao Ridge (CTJ11-10(s) sample) or (a mean composition of) Leg ODP 141 sediments respectively; dashed curve, source contamination of a depleted mantle by the same sediments. Numbers on the curves indicate the mass fraction of sediment component. Diamonds, basalts from Chile Ridge segment 1 (CTJ29); squares, basaltic andesites (CTJ28); dots, basaltic andesites from Taitao Ridge (CTJ11); bold crosses [on Figure 8a only], low-Si North Taitao Canyon dacites (CTJ17), and regular crosses, high-Si CTJ17 dacites; triangles, sediments from the CTJ area. Sr-Nd-O isotopic data are listed in Table 3. Data sources for fields: SCR, Southern Chile Ridge [*Klein and Karsten*, 1995]; AVZ, Austral Volcanic Zone [*Stern and Kilian*, 1996]; SVZ, South Volcanic Zone [*Lopez-Escobar et al.*, 1993]. Chemical and isotopic parameters of the end-members used in the calculation of mixing models are presented in Table 5.

3. Discussion

3.1. Tectonic and Age Constraints on the Sources of CTJ Lavas

[25] Previous investigations in the CTJ region have shown that the subduction of the Chile Ridge since 6 Ma has been coeval with the emplacement of various magmatic suites in the forearc [*Mpodozis et al.*, 1985; *Forsythe et al.*, 1986; *Kaeding et al.*, 1990; *Lagabrielle et al.*, 1994; *Le Moigne et al.*, 1996; *Bourgois et al.*, 1996; *Guivel et al.*, 1999]. These include the Cabo Raper plutonic suite dated at 4.8–5.1 Ma [*Guivel et al.*, 1999], the volcano-sedimentary sequence of the Chile Margin Unit exposed on the Taitao Peninsula and dated from 5.3 to 1.5 Ma [*Bourgois et al.*, 1993], and the volcanic sequence of the Taitao Ridge drilled during ODP Leg 141 at Site 862. Rhyolitic samples from Site 862 provided ages of 1.5–2.2 Ma [*Forsythe et al.*, 1995b]. Our new Ar/Ar ages obtained on the fresh CTJ lavas emphasize the good correlation that exists between the distribution of the magmatic activity in the CTJ area, with the general northward migration of the CTJ along the Chile margin through time (Figure 8). These data confirm previous suggestions that the age of volcanism is getting younger toward the present-day Triple Junction [*Guivel et al.*, 1999; *Lagabrielle et al.*, 2000]. The CTJ28 basaltic andesites which yield the youngest ages (<70 and <127 ka) among the CTJ lava population, are closest to the active Chile spreading segment 1. The CTJ11-6 basaltic andesite located on the Taitao Ridge, 70 km southward from the CJT, provides an older age (1.1 Ma), not very different from those obtained by *Forsythe et al.* [1995b] (1.5–2.2 Ma) on

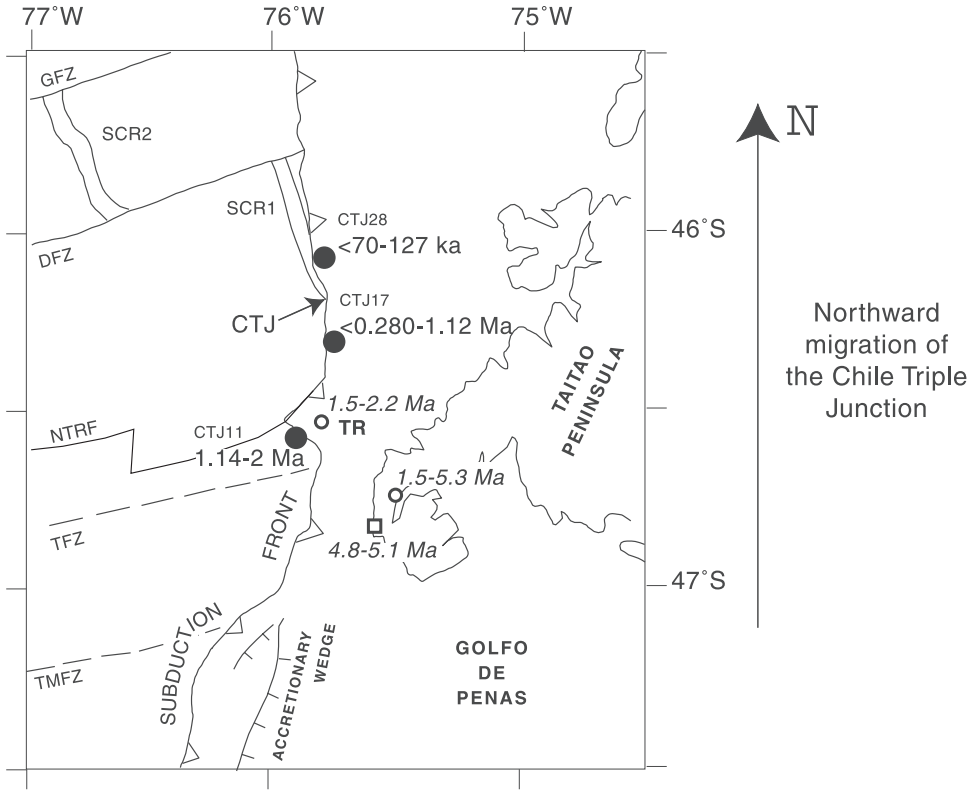

Figure 8. Location of the Pliocene to Quaternary calc-alkaline magmatic rocks in the vicinity of the Chile Triple Junction (CTJ) modified from *Lagabrielle et al.* [2000]. Note the good correlation of magmatic ages older from south to north in agreement with northward migration of the CTJ. Filled circles, new $^{40}Ar/^{39}Ar$ dates on basaltic andesites and dacites from the CTJ lava population obtained by Nicolas Arnaud; empty circles, $^{40}Ar/^{39}Ar$ dates on rhyolitic samples from Leg ODP 141, Site 862 on the Taitao Ridge [*Forsythe et al.*, 1995b], and nannoplankton assemblages ages [*Bourgois et al.*, 2000] from volcanic-sedimentary Chile margin unit on the Taitao Peninsula; empty square, $^{40}Ar/^{39}Ar$ dates on the Cabo Raper granodioritic pluton on the Taitao Peninsula [*Guivel et al.*, 1999]. GFZ, Guamblin Fracture Zone; DFZ, Darwin Fracture Zone; NTRF, North Taitao Ridge Fault; TFZ, Taitao Fracture Zone; TMFZ, Tres Montes Fracture Zone; SCR2 and SCR1, Southern Chile Ridge segment 2 and segment 1, respectively; CTJ, Chile Triple Junction; TR, Taitao Ridge.

rhyolites from the same ridge. The ages of emplacement of high-Si dacites from CTJ17 (less than 1.12 and less than 0.28 Ma), while also young, are not as well constrained as the former.

[26] Considering this spatial and temporal distribution, the CTJ magmatism is clearly related to the interaction between the currently spreading ridge and the thin overlying lithosphere of the upper plate. If we consider the present-day plate configuration and if we assume a 30° dip for the Antarctica slab [*Bourgois et al.*, 1996], the top of the hot descending oceanic crust is presently at a maximum depth of 12 km below all the studied CTJ lavas. This precludes any contribution of the subcontinental mantle, usually considered as the main source of Andean arc magmas, even taking into consideration high rates of tectonic erosion of the Chile margin [*Bourgois et al.*, 1996, 2000]. Consequently, the only sources likely involved in the CTJ magma genesis are: (1) the suboceanic mantle; (2) the young downgoing oceanic crust; (3) the sediments of the accretionary prism; (4) the Chile continental crust; and (5) oceanic materials (basalts, gabbros, and peridotites) possibly underplated tectonically at the base of the Chile continental crust [*Bourgois et al.*, 2000; *Lagabrielle et al.*, 2000].

3.2. Possible Origins of Near-Trench Intermediate and Felsic Magmas

[27] The CTJ magmas are unlikely to derive from large-scale partial melting of continental crust materials or of continent-derived sediments. Indeed, their Sr and Nd isotopic ratios show that the source materials had slightly depleted compositions within the range of those known for the suboceanic Chile Ridge mantle (Figure 7a). Actually, CTJ17 dacites have Sr and Nd isotopic ratios <0.70455 and >0.5128, respectively, while sediments or basement rocks from the CTJ area have $^{87}Sr/^{86}Sr > 0.706$ and $^{143}Nd/^{144}Nd < 0.5125$ (Table 5).

[28] The isotopic variations among the CTJ lavas also preclude a simple closed-system fractionation of an MORB-type magma. Indeed, there is a general enrichment in radiogenic Sr and $\delta^{18}O$ coupled with radiogenic Nd depletion from basalts to dacites (Figure 7). This trend could be a result of AFC, but the complex behavior of some incompatible elements with increasing silica contents indicates

Table 5. Chemical and Isotopic Parameters Used in the Calculation of Mixing Models

Mixing Curves End-Members	Sample	Sr, ppm	$^{87}Sr/^{86}Sr$	Nd, ppm	$^{143}Nd/^{144}Nd$	$\delta^{18}O$
	Source					
Basalt-mantle (this study)	CTJ29-3[a]	128	0.702734	12.00	0.513117	5.77
	Contaminants					
Taitao Ridge sediment covering (this study)	CTJ11-10(s)	290	0.706371	21.50	0.512533	10.48
Sediments Leg ODP141 [*Stern and Kilian*, 1996]		305	0.708000	21.00	0.512400	10.00

[a]Analyses were performed on separated chips of glass.

that either simple fractional crystallization or AFC are not the dominant processes involved in the genesis of intermediate and felsic CTJ magmas. Figure 9 shows N-MORB-normalized incompatible elements and chondrite-normalized REE concentration patterns for representative basaltic to dacitic CTJ lavas. Highly incompatible elements such as LILE and Th increase more or less regularly with increasing silica contents as expected from fractional crystallization. However, the corresponding REE patterns are not parallel and show a general decrease in middle REE (MREE) and HREE concentrations from basalts to dacites (Figure 9). Our attempts to reproduce this REE pattern evolution postulating the fractionation of amphibole and accessory phases such as titanite or apatite were unsuccessful.

[29] The isotopic compositions of the CTJ lavas (Figure 7) require the addition of a ^{18}O- and ^{87}Sr-enriched and a ^{143}Nd-depleted component to a MORB-type source during their genesis. This implies that these rocks might derive from three components: MORB-type mantle, MORB, and sedimentary rocks. The calculated mixing curves shown in Figures 7b and 7c correspond to bulk mixing between (1) a representative N-MORB from the Southern Chile Ridge segment 1 (sample CTJ29-3) and the local sediment CTJ11-10(s) (solid curve, Figure 7b) or the mean composition of Leg ODP 141 sediments (solid curve, Figure 7c), and (2) a theoretical, depleted suboceanic mantle isotopically similar to CTJ29-3 N-MORB but having Sr and Nd concentrations ten times lower, and the same enriched end-member (dashed curves on Figures 7b and 7c).

[30] The first model (solid curves) corresponds to bulk mixing between basaltic magmas and the sediments (or the melts derived from them), whereas the second one approx-

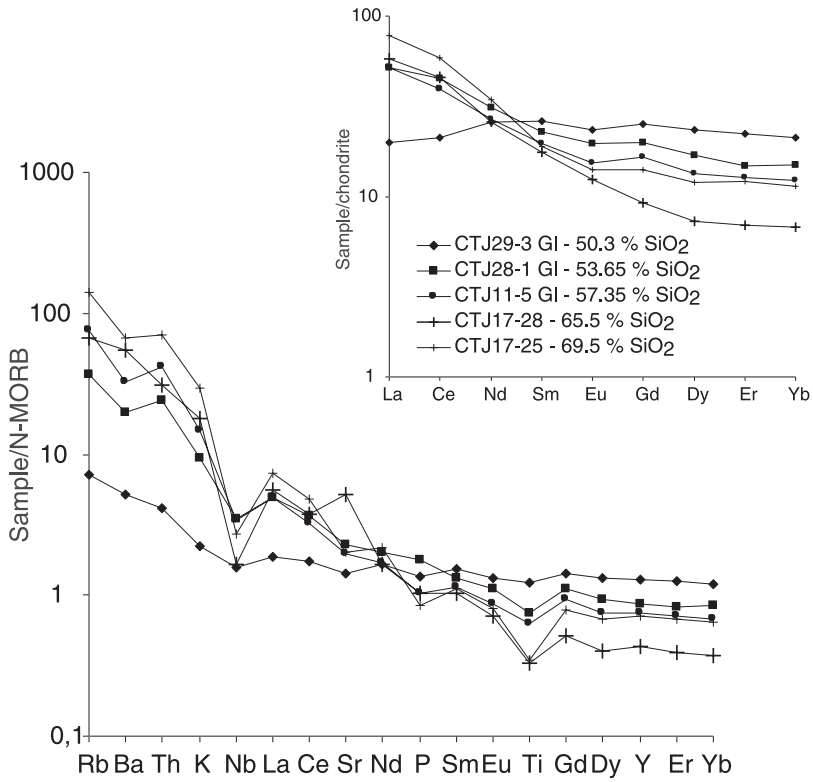

Figure 9. Trace element abundance patterns for representative CTJ lavas, ranging from basalt to dacites, normalized to the composition of N-MORB [*Sun and McDonough*, 1989]. The inset shows rare earth element patterns for the same samples normalized to chondritic values [*Sun and McDonough*, 1989]. The trace element patterns are not parallel and we observe a general decrease in MREE and HREE from basalt to dacites, which is incompatible with fractional crystallization process.

imates the bulk addition of sediments (possibly melted) into the mantle source followed by partial melting of this metasomatized mantle (dashed curves). Clearly, the latter curves do not match the isotopic compositions of the CTJ basaltic andesites and dacites, and thus the hypothesis of melting of metasomatized MORB mantle can be discarded. Despite the scatter in Figures 7b and 7c, the bulk mixing curves fit reasonably well our isotopic data, which suggest that all studied lavas derived from a MORB source through an addition of less than 30% sediments.

[31] Three processes involved in the petrogenesis of the CTJ lavas are consistent with the "bulk mixing" solid curves shown in Figures 7b and 7c:

[32] (1) Crustal contamination/AFC of MORB ascending within the accretionary prism and the Chile continental crust is plausible given the location of the CTJ samples, but this process does not fit with their incompatible trace element features as discussed above.

[33] (2) Melting of a mixture of MORB plus sediments seems also very appropriate in such a tectonic setting and has already been proposed for the Taitao Ridge rhyolites by *Forsythe et al.* [1995a]. Numerous experimental studies have shown that hydrous partial melting of a basaltic protolith produces acidic liquids, and this model will be tested below for the CTJ dacites. However, the compositions of the corresponding experimental melts do not fit with the geochemical features of the CTJ basaltic andesites which contain up to 6.5 wt % MgO. The occurrence in these rocks of magnesian olivine phenocrysts also suggests their derivation from a basaltic liquid.

[34] (3) Magma mixing between basaltic and felsic liquids is an efficient process in creating basaltic andesites, as already shown for the South Volcanic Zone [*Gerlach et al.*, 1988]. The major, trace element and isotopic compositions of the CTJ basaltic andesites are broadly intermediate between those of MORB and CTJ17 dacites from the North Taitao Canyon, and thus might be consistent with an origin through magma mixing between these two compositional end-members. However, various mixing tests involving N-MORB from the Chile Ridge and CTJ17 dacites failed to reproduce at the same time both major and trace element compositions and isotopic Sr-Nd-O compositions. For instance, a mixture of 25% of N-MORB CTJ29-3 with 75% CTJ17-20 dacite reproduces the trace element and Nd isotopic composition of basaltic andesite CTJ11-5 while more than 55% of the N-MORB end-member is needed to match its major element and Sr isotopic compositions. Of course, such mixing may have involved basaltic melts and presently unsampled felsic melts having either trace element patterns or isotopic ratios slightly different from the CTJ dacites. Thus even if our mixing models cannot fully support this process, it is presently impossible to discard it. This hypothesis is also consistent with the common occurrence in the basaltic andesites of olivine phenocrysts more magnesian than those of basalts (Figure 3).

[35] Thus we consider the magma mixing model as the most appropriate for the CTJ basaltic andesites because we know that N-MORB magmas extracted from the mantle of the subducting spreading ridge are available below the continental wedge, as shown from past situations in the Taitao Peninsula and on the Taitao Ridge [*Lagabrielle et al.*, 1994; *Guivel et al.*, 1999]. In the following sections, we demonstrate that felsic liquids are also produced in such context.

3.3. Dacite Genesis: Tests of the Partial Melting of Morb Plus Sediments

[36] Given the configuration of the CTJ region, partial melting of a basaltic protolith at relatively shallow depths can be envisioned. The minimal conditions of hydrous melting for metabasalts in low-pressure conditions are given by the wet basalt solidus of *Green* [1982]. Under pressures lower than 1.5 GPa, these conditions range from 650° to 1000°C and may lead to the production of slab melts in the presence of large amounts of water [*Prouteau et al.*, 1999]. The melting of terrigenous sediments can occur under similar conditions [*Tatsumi*, 2001]. Very low pressure dehydration and water-saturated melting experiments of basaltic to andesitic greenstones and amphibolite were investigated by *Beard and Lofgren* [1991]. These authors show that water-saturated melting occurs between 800° and 1000°C at pressures ranging from 0.1 to 0.7 GPa, and produces silicic melts rather similar to the studied high-Si dacites, coexisting with an amphibole- and plagioclase-rich restite assemblage. Under higher pressures, i.e., within the garnet stability field, numerous studies [*Rapp et al.*, 1991; *Sen and Dunn*, 1994] have demonstrated that the melting of metabasalts produces HREE-depleted felsic melts similar to our low-Si dacites, which have been often referred to as adakites [*Defant and Drummond*, 1990; *Martin*, 1999].

[37] As discussed above, the CTJ high-Si dacites plot along mixing lines between N-MORB from the Chile Ridge and local sediments from the Taitao Ridge (Figure 7b). These features are consistent with the contribution of 25 ± 5% of sediments in the mixture. We have thus tested (model D1) the melting of 75% of typical N-MORB (sample CTJ29-3, Tables 2 and 5) and 25% of local sediments (CTJ11-10(s), Tables 2 and 5) to produce the "high-Si dacites." This model cannot be applied to the low-Si dacites because we lack relevant oxygen isotope data. However, their Sr and Nd isotopic features (Figure 7a) suggest that their source also contains a sedimentary component. Thus regarding the origin of the latter rocks, we have chosen to test (model D2) the melting of a metabasalt identical to the basaltic sample from the Chile Ridge (sample D42-3). This sample shows the strongest subduction-related signature [*Klein and Karsten*, 1995]. It has been considered by these authors to have been derived from the melting of depleted mantle source, contaminated at depth by altered oceanic crust and sediments.

[38] Mass balance calculations on major elements permit evaluation of the degrees of melting and restite assemblages for both high-Si and low-Si dacites (models D1 and D2, respectively). Major element compositions of the minerals and rocks used for mass balance calculations are presented in Tables 6 and 7, respectively. Model D1 final composition is that of CTJ17-12 sample and model D2 final composition of that of CTJ17-28. Results of mass balanced calculations are presented in Table 8. CTJ17-12 high-Si dacite is modeled by partial melting of ca. 32% of source D1 (75% MORB + 25% sediments) with a residue of 60.4% amphibole + 34.5% plagioclase (An70) + 4.6% magnetite and 0.5% apatite. The best result approximating the composition of the CTJ17-28 low-Si dacite is ca. 20% partial melting of

Table 6. Major Element Compositions of the Minerals Used for the Mass Balance Calculations

	Hornblende	Plagioclase An80	Plagioclase An70	Garnet	Ilmenite	Magnetite	Apatite
SiO_2	47.50	48.72	50.45	38.54		0.15	0.09
TiO_2	2.27	0.04			52.73	8.23	
Al_2O_3	8.09	31.79	31.37	24.28		0.38	
Fe_2O_3*[a]	13.61	0.42	0.26	15.91	44.65	90.15	0.23
MnO	0.16			0.36	0.61	0.43	0.1
MgO	14.98		0.2	13.05	1.78	0.54	0.02
CaO	11.29	16.56	14.37	7.86	0.23	0.1	56.15
Na_2O	1.81	2.43	3.17				0.11
K_2O	0.3	0.05	0.18			0.2	
P_2O_5							43.3

[a]Total Fe as Fe_2O_3.

source D2 coexisting with a residue rich in amphibole and plagioclase, and containing also garnet + ilmenite + apatite.

[39] We have tested the major element-based models with the abundance systematics of the REE and other trace element compositions. Mineral/liquid partition coefficients used for partial melting calculations come from *Martin* [1987] and references therein, with the exception of K_{liq}^{Garnet} for Ba and Nb [*Arth*, 1976 and *Johnson*, 1994, respectively] and $K_{liq}^{Ilmenite}$ for Nb [*Green and Pearson*, 1987]. The results of batch partial melting modeling [*Shaw*, 1970] are presented in Figure 10 which compares the REE and trace element patterns of the two groups of dacites with the calculated patterns. The presence of small amounts of garnet in the melting residue for D2 model is consistent with the low-HREE contents of the low-Si dacites. The lower abundance of plagioclase in the residue of model D2 is consistent with the higher Sr content and lack of a negative Eu anomaly in the low-Si dacite group. The main discrepancy between the compositions of calculated liquids and low-Si CTJ dacites (calculated using model D2) is that the former are too depleted in HREE with respect to the latter, suggesting that <6% of residual garnet was involved in the genesis of low-Si dacites. However, given the numerous uncertainties in the parameters used for partial melting calculations (source compositions, partial melting rates, partition coefficients, and mineral compositions of the residues), we will consider hereafter that these models provide a reasonable fit with our natural melts. Of course, the validity of these melting models requires also that the thermodynamic and chemical conditions (T, P, and H_2O content) necessary for melting were matched below the near-trench CTJ area, which will be discussed below.

Table 7. Major Element Compositions of the Possible Sources Used for Mass Balanced Calculations[a]

	Source D1, Mixing of Basalt B and Sediment S (25% S + 75% B)	Source D2, Basalt (D42-4 [*Klein and Karsten*, 1995])
SiO_2	53.8	50.45
TiO_2	1.39	1.18
Al_2O_3	15.49	15.91
Fe_2O_3*[b]	9.54	9.14
MnO	0.15	0.15
MgO	6.59	8.16
CaO	9.31	11.62
Na_2O	2.99	2.77
K_2O	0.56	0.44
P_2O_5	0.18	0.17
LOI		
Total	100	100

[a]Model D1 concerns high-Si dacites petrogenesis and according to their isotopic composition, the high-Si dacite source composition is a mixing of 25% of sediment (CTJ11-10s, Table 2) and 75% of basalt (CTJ29-3, Table 2). The source composition used for partial melting modeling D2 concerning low-Si dacites CTJ17 petrogenesis, is a basalt from the Chile Ridge segment [sample D42-3, *Klein and Karsten*, 1995]. This basalt has isotopic and trace element composition characteristic of arc magmas.

[b]Total Fe as Fe_2O_3.

3.4. *P-T*-H_2O Conditions of Melting

[40] Our results demonstrate that low- and high-Si dacites originated from hydrous melting of a metabasaltic protolith plus sediment. The most striking difference between these two types of magmas is that residual garnet is involved in the genesis of the low-Si dacites, implying variable pressures of melting.

[41] The availability of important amounts of water at shallow depths in the CTJ area is not a major restriction in our opinion. Three sources of water can be involved: (1) the water stored in the sedimentary pile within the accretionary prism [*Behrmann et al.*, 1994]; (2) water from the altered oceanic basalts; and (3) water from serpentinized peridotites, e.g., those exposed at the base of the Bahia Barrientos ophiolite on the Taitao Peninsula. During subduction of very young oceanic crust, water is released at shallow depths along the thrust interface [*Harry and Green*, 1999], and the corresponding fluids might uprise along the detachment into the accretionary prism.

[42] Thermal effects of ridge subduction can be inferred from a simple numerical model by *Iwamori* [2000]. Its application to the CTJ case shows that maximum temperatures ranging from 600° to 780°C are attained at the interface between the subducted slab and the overlying arc

Table 8. Results of Mass Balanced Calculations for Partial Melting Modeling[a]

	D1 Model	D2 Model
r^2	0.252	0.945
F, %	31.8	19.6
Modal composition		
Hornblende, %	60.43	63
Plagioclase An80, %		29.1
Plagioclase An70, %	34.46	
Garnet, %		6
Ilmenite, %		0.8
Magnetite, %	4.64	
Apatite, %	0.46	1.1

[a]Parameters obtained: F, partial melting rate; r^2, the sum of squares of the residuals; modal composition of the residue.

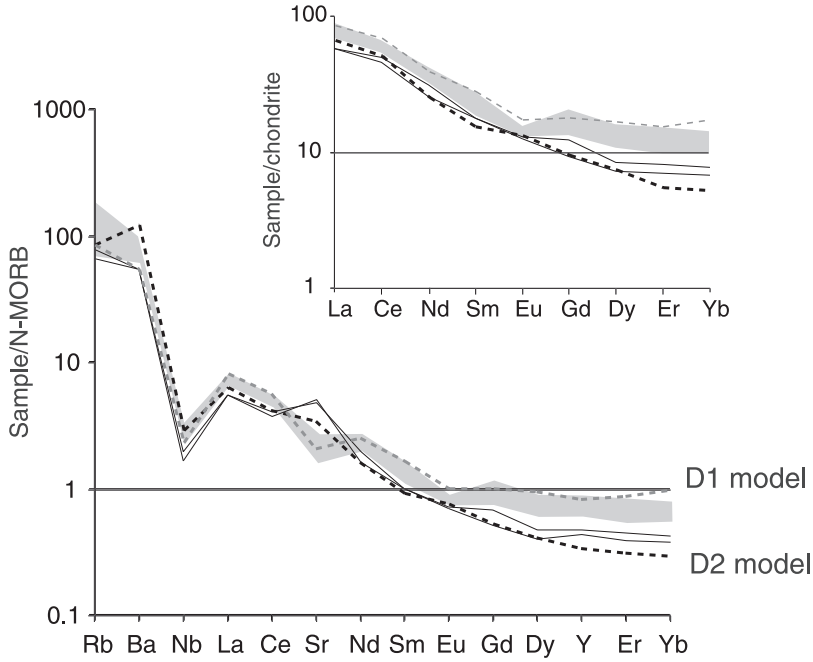

Figure 10. Trace element and rare earth element patterns normalized to N-MORB and chondrite abundances, respectively [*Sun and McDonough*, 1989] of calculated partial melts, compared with natural CTJ17 dacitic lavas. Model D1 melt composition (shaded dashed line) matches those of the calc-alkaline, high-Si CTJ17 dacites (shaded area) while model D2 melt composition (bold dashed line) broadly reproduces those of adakite-like, low-Si CTJ17 dacites (thin line).

crust for depths of 15–30 km. We can even expect in the CTJ case, a thermal regime much hotter than that predicted by the *Iwamori*'s [2000] models because of the succession in the studied area of several events of ridge subduction due to the segmentation of the Chile Ridge (the blowtorch effect of *DeLong et al.* [1979]), as discussed in the work of *Lagabrielle et al.* [2000].

[43] High-Si dacite melts likely originate from a pressure domain where plagioclase and amphibole are stable but garnet unstable ($P < 0.8$ GPa), corresponding to depths shallower than 25 km and a temperature field ranging from 650° to 900°C [*Green*, 1982; *Schmidt and Poli*, 1998]. Low-Si dacite melts originate in a pressure field where both garnet and plagioclase are stable, that is, according to the same authors between 0.8 and 1.5 GPa corresponding to depths ranging from 25 to 45 km and temperatures ranging from 650° to 800°C. At present, the CTJ17 dacites are localized only 8 km landward from the trench. Postulating their derivation from the sommital part of the oceanic crust (where basalts and sediments occur together), followed by vertical ascent of the liquids, leads to conclude that the top of the slab should be at a maximum depth of only 5 km under the CTJ17 dredge site. This is inconsistent with the minimum depth of 25 km required for the genesis of the low-Si dacites according to experimental data.

3.5. Tectonic Conditions of Melting

[44] The most simple explanation accounting for the emplacement at the trench of low-Si dacitic magmas formed at a minimum depth of 25 km is that they have been channelized along the thrust plane during their ascent. Indeed, the top of the subducting slab is in extensional regime at low depths [*Hasegawa et al.*, 1994] and open fractures are likely to occur in such a context. In addition, studies have suggested that hydrous fluids are accumulated and channeled along the decollement plane [*Bangs et al.*, 1999]. This hypothesis provides an elegant explanation to the presence in the same dredge CTJ17 of high-Si and low-Si dacites. However, it seems very unlikely that viscous dacitic magmas could travel tens of kilometers along the thrust plane without being quenched by the hydrous fluids percolating concomitantly.

[45] Alternative explanations involve tectonic processes, which might have resulted in changes of the geometry of the triple junction during the last mega-year, allowing dacitic magmas to be exposed within the trench today. A previous tectonic study of the synsubduction Chile margin segment [*Bourgois et al.*, 2000] has documented the highly complex morphology and history of this segment during the past 1 Ma. This evolution includes episodes of subduction-accretion and subduction-erosion, as well as a possible oceanward ridge jump of part of the Southern Chile Ridge segment 1 and fragmentation of the oceanic lithosphere. Thus 1 or 2 Ma ago, the plate configuration at the CTJ area might have been different from today (Figure 2), which implies that the studied lavas may not be anymore in their right original location with respect to the trench.

[46] We propose two different hypothetical models that might account for the development of very specific *P-T* field conditions leading to the genesis of high-Si and low-Si dacites, ca. 1 Ma ago in the CTJ region. The first one implies rapid tectonic erosion, as documented earlier in such geodynamic contexts [*Bourgois et al.*, 2000; *Bourgois and Michaud*, 2002]. The second one involves rapid slab bend-

ing right below the trench. Both models lack geological and geophysical support and we are well aware that none of them can be considered as a single, definite solution.

3.5.1. Tectonic Model Implying High Rates of Tectonic Erosion

[47] The high-Si dacites have likely been formed under low-pressure conditions, at ca. 15–20 km depth. This condition implies a minimum landward retreat of the trench axis of 18 km during the past 0.3–1.12 Ma, i.e., a minimum continental margin retreat rate of 16 km/Ma. In the same way, the low-Si adakite-like dacites have been formed within the plagioclase and garnet stability field at ca. 25 km depth or more. Their age is not constrained but admitting a slab dip of 30°, they are likely to have been emplaced at least 50 km landward from the trench. The 16 km/Ma rate is much higher than the 5.5–7.5 km/Ma invoked during the last 3–4.2 Ma in the case of the Cabo Raper pluton on the Taitao Peninsula [*Bourgois et al.*, 1996]. However, it has been proposed that the geometry of the CTJ trench area changed significantly during the Quaternary, in response to highly variable glacial-interglacial sediment supply [*Bourgois et al.*, 2000]. Recent subduction of the Chile Ridge is therefore characterized by very high rates of frontal erosion that removed most of the previously accumulated accretionary prism in 160 ka but also by active subduction erosion at depths consistent with the narrowness of the continental slope along the margin north of the triple junction. The tectonic context of the CTJ is also characterized by strike-slip faulting [*Lagabrielle et al.*, 2000] and ridge jump [*Bourgois et al.*, 2000]. Combination of these tectonic processes associated with tectonic erosion could explain a rapid landward migration of the trench axis as illustrated in Figure 11. One mega-annum ago, the slab could have been 30 km below what is "presently" the near-trench area. Subducting oceanic crust metamorphosed into the greenschist to garnet-bearing amphibolite facies may have been partially remelted at depths ranging from 20 to 30 km producing the high-Si and low-Si dacitic melts, respectively. From 1 to ca. 0.3 Ma, melting of the subducting oceanic crust or of tectonic slices of oceanic crust underplated at the base of the accretionary prism may have been associated with tectonic erosion that removed considerable volume of the continental margin, allowing the young dacitic melts to be exposed within the trench today. This model is also close to that developed for the origin of the rhyolites drilled from the Taitao Ridge during ODP Leg 141, Site 862 [*Forsythe et al.*, 1995a], with the difference that these authors do not consider contribution of sediments.

3.5.2. Tectonic Model Implying a Complex Vertical Slab Geometry

[48] The previous model implies considerable rates of tectonic erosion. This second model has been developed with the aim of minimizing the required rates of tectonic-erosion. We propose that parts of the slab should be buried rapidly to depths of 20–30 km right under the trench. This model is based on the fact that the oceanic lithosphere entering the trench at the CTJ is characterized by the occurrence of a group of transform faults. This feature has already been recognized as an important constraint leading to abnormal volcanism in the CTJ region [*Mpodozis et al.*, 1985; *Kaeding et al.*, 1990; *Nelson et al.*, 1993; *Le Moigne et al.*, 1996; *Bourgois et al.*, 1993; *Lagabrielle et al.*, 1994; *Bourgois et al.*, 1996]. In our second model (Figure 12), transform faults are considered as stress-free boundaries that allow the partitioning of the slab into successive independent portions. We assume that the youngest slab portions may bend drastically in response to mantle counterflow in

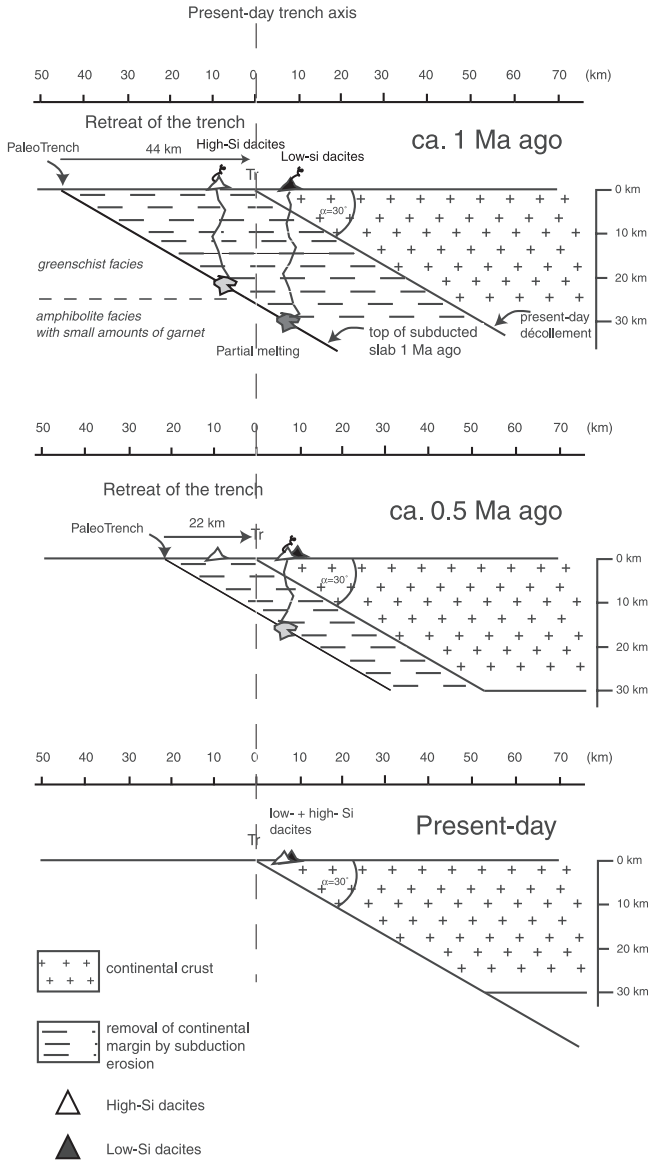

Figure 11. Geodynamical model based on high rates of subduction erosion: possible evolution of the Chile continental margin during last 1 Ma. Quaternary calc-alkaline and adakite-like dacites have been collected during CTJ cruise only 8 km landward from the trench axis. Only an association of high rates of tectonic erosion and partial melting of the subducting slab at depths ranging from 20 to 30 km may allow young CTJ dacitic magmas to be exposed within the trench at the present day. Partial melting at various depths ranging from 15 to 30 km of the subducting oceanic crust + sediments metamorphosed within the greenschist to garnet-bearing amphibolite facies products the high-Si and low-Si dacitic magmas while subduction of the Chile Ridge induces removal of the forearc material at depths. Tr, present-day trench axis.

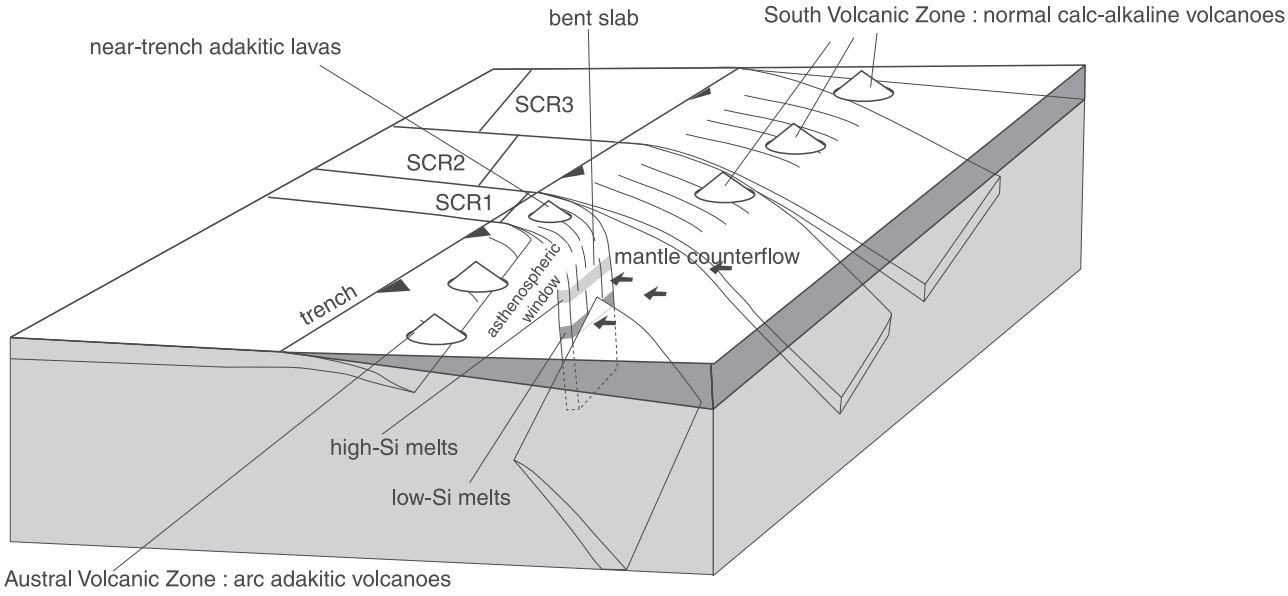

Figure 12. Geodynamical model based on vertical slab geometry: as in Figure 11, near-trench dacitic magmatism on the Chile triple junction derives from the melting of a basaltic protolith plus sediment at various depths. Only a configuration with an almost vertical slab may lead to the presence of two groups of dacites emplaced in the same site (see text for dicussion).

the mantle wedge, moving from the back arc to the trench. Such a bending might allow portion of relatively young and still hot oceanic crust to reach rapidly depths of 20–30 km. The CTJ region is unfortunately devoid of significant seismicity and seismological data are not available in order to constrain the dip of slab under the CTJ. As a consequence, this model remains hypothetical.

4. Conclusion

[49] (1) The CTJ basaltic andesites and dacites provide the first Quaternary example of magmas carrying subduction-related signatures being emplaced in the forearc domain, less than 20 km away from the active Chile trench. The petrogenetic models developed in the present study may thus provide insights into a number of apparently similar processes throughout the geological record [*DeLong et al.*, 1979].

[50] (2) The present-day very shallow depth (<12 km) of the top of the subducted oceanic plate below the CTJ area excludes any contribution from the subarc mantle to the genesis of the studied lavas, and the isotopic features of the andesitic and dacitic liquids are inconsistent with an origin through simple anatectic melting of the upper continental crust or of the local terrigenous sediments.

[51] (3) The basaltic andesites from dredges CTJ28 and CTJ11 can result from mixing between the basaltic and low-Si dacitic magmas.

[52] (4) In our preferred model, the most likely sources of the dacites are the downgoing basaltic oceanic crust plus variable amounts of associated sediments.

[53] (5) The high-Si dacites are best explained by water-saturated melting of a mixture of 75% MORB + 25% sediments at 800°–900°C under low pressures. Although they are relatively depleted in HREE due to the presence of amphibole in the residue, they do not present the typical features of slab melts (adakites). Their genesis in high-temperature and low-pressure conditions [*Beard and Lofgren*, 1991] allows us to consider them as an analog of the Early Archean granitoids [*Martin*, 1987, 1999; *Martin and Moyen*, 2002].

[54] (6) The low-Si dacites are adakite-like magmas, and can be modelled as a result of hydrous melting of the Chile Ridge basalts (which already carry a subduction signature) provided that they were previously metamorphosed into the garnet amphibolite facies. We attribute the presence of such rocks at presently shallow depths to short-lived changes in the geometry of the triple junction, possibly due to a combination of subduction-erosion and strike-slip tectonics or rapid slab bending right below the trench.

[55] (7) The very unusual tectonic context of the CTJ, which involved the successive subduction of several ridge segments below the same zone, was able to produce the quite exceptional conditions of melting required for the above models: temperatures of 700°–900°C at depths ca. 15–30 km. Such conditions, rarely realized in modern subduction environments, may provide a clue to the understanding of Archean magmatic processes.

[56] **Acknowledgments.** We thank R. Arculus, an anonymous reviewer and JGR Associate Editor V. Bennett whose comments and suggestions greatly improved this manuscript. F. Martineau's help in the O isotopic measurements is also acknowledged. The CTJ cruise was supported by IFREMER (France). We thank the captain and the crew of the R/V *L'Atalante* for their efficient work and the Servicio Hidrografico y Oceanografico (SHOA) de la Armada de Chile.

References

Aguillón-Robles, A., T. Calmus, M. Benoit, H. Bellon, R. C. Maury, J. Cotten, J. Bourgois, and F. Michaud, Late Miocene adakites and Nb-enriched basalts from Vizcaino Peninsula, Mexico: Indicators of East Pacific Rise subduction below southern Baja California?, *Geology*, *29*, 531–534, 2001.

Arculus, R. J., Aspects of magma genesis in arcs, *Lithos*, *33*, 189–208, 1994.

Arth, J. G., Behaviour of trace elements during magmatic processes—A summary of theoretical models and their applications, *J. Res. U.S. Geol. Surv.*, *4*, 41–47, 1976.

Bangs, N. L. B., T. H. Shipley, J. C. Moore, and G. F. Moore, Fluid accumulation and channeling along the northern Barbados Ridge decollement thrust, *J. Geophys. Res.*, *104*, 20,399–20,414, 1999.

Barker, F., G. L. Farmer, R. A. Ayuso, G. Plafker, and J. S. Lull, The 50 Ma granodiorite of the eastern Gulf of Alaska: Melting in an accretionary prism in the forearc, *J. Geophys. Res.*, *97*, 6757–6778, 1992.

Beard, J. S., and G. E. Lofgren, Dehydration-melting and water-saturated melting of basaltic and andesitic greenstones and amphibolites at 1, 3 and 6.9 kb, *J. Petrol.*, *32*, 365–401, 1991.

Behrmann, J. S., S. D. Leslie, S. C. Cande, and ODP Leg 141 Scientific Party, Tectonics and geology of spreading ridge subduction at the Chile Triple Junction: A synthesis of results from Leg 141 of the Ocean Drilling Program, *Geol. Rundsch.*, *83*, 832–852, 1994.

Benoit, M., A. Aguillon-Robles, T. Calmus, R. C. Maury, H. Bellon, J. Cotten, J. Bourgois, and F. Michaud, Geochemical diversity of late Miocene volcanism in southern Bala California, Mexico: Implication of mantle and crustal sources during the opening of an asthenospheric window, *J. Geol.*, *110*, 627–648, 2002.

Bourgois, J., and F. Michaud, Comparison between the Chile and Mexico triple junction areas substantiates slab window development beneath northwestern Mexico during the past 12-10 Myr, *Earth Planet. Sci. Lett.*, *201*, 35–44, 2002.

Bourgois, J., Y. Lagabrielle, J. Le Moigne, O. Urbina, M. C. Janin, and P. Beuzart, Preliminary results of a field study of the Taitao ophiolite (Southern Chile): Implications for the evolution of the Chile Triple Junction, *Ofioliti*, *18*, 113–129, 1993.

Bourgois, J., H. Martin, Y. Lagabrielle, J. Le Moigne, and J. Frutos Jara, Subduction erosion related to spreading-ridge subduction: Taitao Peninsula (Chile margin triple junction area), *Geology*, *24*, 723–726, 1996.

Bourgois, J., C. Guivel, Y. Lagabrielle, T. Calmus, J. Boulègue, and V. Daux, Glacial-interglacial trench supply variation, spreading-ridge subduction, and feedback controls on the Andean margin development at the Chile Triple Junction area (45–48°S), *J. Geophys. Res.*, *105*, 8355–8386, 2000.

Cande, S. C., and R. B. Leslie, Late Cenozoic tectonics of the southern Chile trench, *J. Geophys. Res.*, *91*, 471–496, 1986.

Clayton, R. N., and T. K. Mayeda, The use of bromine pentafluoride in the extraction of oxygen from oxides and silicates for isotopic analysis, *Geochim. Cosmochim. Acta*, *27*, 43–52, 1963.

Cole, R. B., and A. R. Basu, Middle tertiary volcanism during ridge-trench interactions in western California, *Science*, *258*, 793–796, 1992.

Cole, R. B., and A. R. Basu, Nd-Sr isotopic geochemistry and tectonics of ridge subduction and middle Cenozoic volcanism in western California, *Geol. Soc. Am. Bull.*, *107*, 167–179, 1995.

Cotten, J., A. Le Dez, M. Bau, M. Caroff, R. C. Maury, P. Dulski, S. Fourcade, M. Bohn, and R. Brousse, Origin of anomalous rare-earth element and yttrium enrichments in subaerially exposed basalts: Evidence from French Polynesia, *Chem. Geol.*, *119*, 115–138, 1995.

Dalrymple, G. B., and M. A. Lanphere, $^{40}Ar/^{39}Ar$ age spectra of some undisturbed terrestrial samples, *Geochim. Cosmochim. Acta*, *38*, 715–738, 1974.

Defant, M. J., and M. S. Drummond, Derivation of some modern arc magmas by melting of young subducted lithosphere, *Nature*, *347*, 662–665, 1990.

Defant, M. J., M. Richerson, J. Z. de Boer, R. H. Stewart, R. C. Maury, H. Bellon, M. S. Drummond, M. D. Feigenson, and T. E. Jackson, Dacite genesis via both slab melting and differentiation: Petrogenesis of La Yeguada Volcanic Complex, Panama, *J. Petrol.*, *32*, 1101–1142, 1991.

DeLong, S. E., W. M. Schwarz, and R. N. Anderson, Thermal effects of ridge subduction, *Earth Planet. Sci. Lett.*, *44*, 239–246, 1979.

DeMets, C., R. G. Gordon, D. F. Argus, and S. Stein, Current plate motions, *Geophys. J. Int.*, *101*, 425–478, 1990.

DePaolo, D. J., *Neodymium Isotope Geochemistry: An Introduction*, Springer-Verlag, New York, 1988.

Dickinson, W. R., and W. S. Snyder, Geometry of triple junctions related to San Andreas transform, *J. Geophys. Res.*, *84*, 561–572, 1979.

Faure, G., *Principles of Isotope Geology*, 2nd ed., John Wiley, Hoboken, N.J., 1986.

Forsythe, R., E. Nelson, M. Carr, M. Kaeding, M. Herve, C. Mpodozis, J. Soffia, and S. Harambour, Pliocene near-trench magmatism in southern Chile: A possible manifestation of ridge collision, *Geology*, *14*, 23–27, 1986.

Forsythe, R. D., J. K. Meen, J. F. Bender, and D. Elthon, Geochemical data of volcanic rocks and glasses recovered from Site 862: Implications for the origin of the Taitao Ridge, Chile Triple Junction region, *Proc. Ocean Drill. Program Sci. Results*, *141*, 331–348, 1995a.

Forsythe, R. D., R. Drake, and R. Olsson, Data report: $^{40}Ar/^{39}Ar$ and additional paleontologic age constraints, Site 862, Taitao Ridge, *Proc. Ocean Drill. Program Sci. Results*, *141*, 421–426, 1995b.

Fourcade, S., R. C. Maury, M. J. Defant, and F. McDermott, Mantle metasomatic enrichment arc crust contamination in the Philippines: Oxygen isotope study of Batan ultramafic nodules and northern Luzon arc lavas, *Chem. Geol.*, *114*, 199–215, 1994.

Gerlach, D. C., F. A. Frey, H. Moreno-Roa, and L. Lopez-Escobar, Recent volcanism in the Puyehue-Cordon Caulle region, southern Andes, Chile (40.5°S): Petrogenesis of evolved lavas, *J. Petrol.*, *29*, 333–382, 1988.

Green, T. H., Anatexis of mafic crust and high pressure crystallization of andesite, in *Andesites*, edited by R. S. Thorpe, pp. 466–487, John Wiley, Hoboken, N.J., 1982.

Green, T. H., and N. J. Pearson, An experimental study of Nb and Ta partitioning between Ti-rich minerals and silicate liquids at high pressure and temperature, *Geochim. Cosmochim. Acta*, *51*, 55–62, 1987.

Guivel, C., J. Bourgois, S. Fourcade, Y. Lagabrielle, H. Martin, and R. C. Maury, New constraints for the origin of ridge-subduction-related plutonic and volcanic suites at the Chile Triple Junction (Taitao Peninsula and Site 862, Leg ODP 141 on the Taitao Ridge), *Tectonophysics*, *311*, 83–111, 1999.

Harris, N., V. Sisson, J. Wright, and T. Palvis, Evidence for Eocene mafic underplating during fore-arc intrusive activity, eastern Chugach Mountains, Alaska, *Geology*, *24*, 263–266, 1996.

Harry, D. L., and N. L. Green, Slab dehydration and basalt petrogenesis in subduction systems involving very young oceanic lithosphere, *Chem. Geol.*, *160*, 309–333, 1999.

Hasegawa, A., S. Horiuchi, and N. Umino, Seismic structure of the northeastern Japan convergent margin: A synthesis, *J. Geophys. Res.*, *99*, 22,295–22,311, 1994.

Haeussler, P. J., D. Bradley, R. Goldfarb, L. Snee, and C. Taylor, Link between ridge subduction and gold mineralization in southern Alaska, *Geology*, *23*, 995–998, 1995.

Hibbard, J. P., and D. E. Karig, Structural and magmatic responses to spreading ridge subduction: An example from SW Japan, *Tectonics*, *9*, 207–230, 1990.

Iwamori, H., Thermal effects of ridge subduction and its implications for the origin of granitic batholith and paired metamorphic belts, *Earth Planet. Sci. Lett.*, *181*, 131–144, 2000.

Johnson, C. M., and J. R. O'Neil, Triple junction magmatism: A geochemical study of Neogene volcanic rocks in western California, *Earth Planet. Sci. Lett.*, *71*, 214–262, 1984.

Johnson, K. T. M., Experimental cpx/and garnet/melt partitioning of REE and other trace elements at high pressures: Petrogenetic implications, Goldschmidt Conference Edinburgh, *Mineral. Mag.*, *58A*, 454–455, 1994.

Kaeding, M., R. D. Forsythe, and E. P. Nelson, Geochemistry of the Taitao ophiolite and near-trench intrusions from the Chile Margin Triple Junction, *J. S. Am. Earth Sci.*, *3*, 161–177, 1990.

Kiminami, K., S. Miyashita, and K. Kawabata, Ridge collision and in situ greenstones: An example from the Late Cretaceous Ryukyu Islands and southwest Japan margin, *Isl. Arc*, *3*, 103–111, 1994.

Klein, E., and J. Karsten, Ocean-ridge basalts with convergent-margin affinities from the Chile Ridge, *Nature*, *374*, 52–57, 1995.

Lagabrielle, Y., J. Le Moigne, R. C. Maury, J. Cotten, and J. Bourgois, Volcanic record of the subduction of an active spreading ridge, Taitao Peninsula (southern Chile), *Geology*, *22*, 515–518, 1994.

Lagabrielle, Y., C. Guivel, J. Bourgois, S. Fourcade, and H. Martin, Magmatic-tectonic effects of high thermal regime at the site of active ridge subduction: The Chile Triple Junction model, *Tectonophysics*, *326*, 255–268, 2000.

Lanphere, M. A., and H. Baadsgaard, Precise K-Ar, $^{40}Ar/^{39}Ar$, Rb-Sr and U/Pb mineral ages from the 27.5 Ma Fish Canyon Tuff reference standard, *Chem. Geol.*, *175*, 653–671, 2001.

Le Maître, R. W., et al., *A Classification of Igneous Rocks and Glossary of Terms*, Blackwell, Malden, Mass., 1989.

Le Moigne, J., Y. Lagabrielle, H. Whitechurch, J. Girardeau, J. Bourgois, and R. C. Maury, Petrology and geochemistry of the ophiolitic and volcanic suites of the Taitao Peninsula-Chile Triple Junction, *J.S. Am. Earth Sci.*, *9*, 43–58, 1996.

Leslie, R. B., Cenozoic tectonics of southern Chile: Triple junction migration, ridge subduction, and forearc evolution, Ph.D. thesis, Columbia Univ., New York, 1986.

Lopez-Escobar, L., R. Kilian, P. D. Kempton, and M. Tagiri, Petrography and geochemistry of Quaternary rocks from the southern volcanic zone of the Andes between 41°30′ and 46°00′S, Chile, *Rev. Geol. Chile*, *20*, 33–55, 1993.

Lytwyn, J., J. Casey, S. Gilbert, and T. Kusky, Arc-like mid-ocean ridge basalt formed seaward of a trench-forearc system just prior to ridge sub-

duction: An example from subaccreted ophiolites in southern Alaska, *J. Geophys. Res.*, *102*, 10,225–10,243, 1997.
Lytwyn, J., S. Lockhart, J. Casey, and T. Kusky, Geochemistry of near-trench intrusives associated with ridge subduction, Seldovia Quadrangle, southern Alaska, *J. Geophys. Res.*, *105*, 27,957–27,978, 2000.
Maeda, J., and H. Kagami, Interaction of a spreading ridge and an accretionary prism: Implications for MORB magmatism in the Hidaka magmatic zone, Hokkaido, Japan, *Geology*, *24*, 31–34, 1996.
Marshak, R. S., and D. E. Karig, Triple junctions as a cause for anomalously near-trench igneous activity between the trench and volcanic arc, *Geology*, *5*, 233–236, 1977.
Martin, H., Petrogenesis of archean trondhjemites, tonalites and granodiorites from eastern Finland: Major and trace element geochemistry, *J. Petrol.*, *28*, 921–953, 1987.
Martin, H., Adakitic magmas: Modern analogues of Archean granitoids, *Lithos*, *46*, 411–429, 1999.
Martin, H., and J.-F. Moyen, Secular changes in TTG composition as markers of the progressive cooling of the Earth, *Geology*, *30*, 319–322, 2002.
Maury, R. C., F. G. Sajona, M. Pubellier, H. Bellon, and M. J. Defant, Fusion de la croûte océanique dans les zones de subduction/collision récentes: L'exemple de Mindanao (Philippines), *Bull. Soc. Geol. Fr.*, *167*(5), 579–595, 1996.
Miyashiro, A., Volcanic rock series in island arcs and active continental margins, *Am. J. Sci.*, *274*, 321–355, 1974.
Morimoto, N., J. Fabries, A. K. Ferguson, I. V. Ginzburg, M. Ross, F. A. Seifert, J. Zussman, K. Aoki, and G. Gottardi, Nomenclature of pyroxenes, *Mineral Mag.*, *52*, 535–550, 1988.
Mpodozis, C., M. Herve, C. Nasi, J. Soffia, R. Forsythe, and E. Nelson, El magmatismo plioceno de Peninsula Tres Montes y su relacion con la evolucion del Punto Triple de Chile Austral, *Rev. Geol. Chile*, *25–26*, 13–28, 1985.
Nelson, E., R. Forsythe, J. Diemer, M. Allen, and O. Urbino, Taitao ophiolite: A ridge collision ophiolite in the forearc of southern Chile (46°S), *Rev. Geol. Chile*, *20*, 137–165, 1993.
Osozawa, S., and T. Yoshida, Arc-type and intraplate-type ridge basalts formed at the trench-trench-ridge triple junction: Implications for the extensive sub-ridge mantle heterogeneity, *Isl. Arc*, *6*, 197–212, 1997.
Pin, C., and J.-L. Paquette, A mantle-derived bimodal suite in the Hercynian Belt: Nd isotope and trace element evidence for a subduction-related rift origin of the Late Devonian Brévenne metavolcanics, Massif Central (France), *Contrib. Mineral. Petrol.*, *129*, 222–238, 1997.
Prouteau, G., B. Scaillet, M. Pichavant, and R. C. Maury, Fluid-present melting of oceanic crust in subduction zones, *Geology*, *27*, 1111–1114, 1999.
Rapp, R. P., E. B. Watson, and C. F. Miller, Partial melting of amphibolite/eclogite and the origin of Archean trondjhemite and tonalites, *Precambrian Res.*, *51*, 1–25, 1991.
Rogers, G., A. D. Saunders, D. J. Terrell, S. P. Verma, and G. F. Marriner, Geochemistry of Holocene volcanic rocks associated with ridge subduction in Baja California, Mexico, *Nature*, *315*, 389–392, 1985.
Schmidt, M. W., and S. Poli, Experimentally based water budgets for dehydrating slabs and consequences for arc magma generation, *Earth Planet. Sci. Lett.*, *163*, 361–379, 1998.
Sen, C., and T. Dunn, Dehydration melting of a basaltic composition amphibolite at 1.5 and 2.0 GPa: Implications for the origin of adakites, *Contrib. Mineral. Petrol.*, *117*, 394–409, 1994.
Sharma, M., A. Basu, R. Cole, and P. DeCelles, Basalt-rhyolite volcanism by MORB-continental crust interaction: Nd, Sr-isotopic and geochemical evidence from southern San Joaquin Basin, California, *Contrib. Mineral. Petrol.*, *109*, 159–172, 1991.
Shaw, D. W., Trace element fractionation during anatexis, *Geochim. Cosmochim. Acta*, *34*, 237–243, 1970.
Sheppard, S. M. F., and C. Harris, Hydrogen and oxygen isotope geochemistry of Ascension Island lavas and granites: Variation with crustal fractionation and interaction with seawater, *Contrib. Mineral. Petrol.*, *91*, 74–81, 1985.
Sherman, S. B., J. L. Karsten, and E. M. Klein, Petrogenesis of axial lavas from the southern Chile Ridge: Major element constraints, *J. Geophys. Res.*, *102*, 14,963–14,990, 1997a.
Sherman, S. B., J. L. Karsten, and E. M. Klein, Enrichment processes in southern Chile Ridge lavas: Constraints from Cl, F, and H_2O, *Eos Trans. AGU*, *78*(46), Fall Meet. Suppl., F825, 1997b.
Stern, C. R., and R. Kilian, Role of the subducted slab, mantle wedge and continental crust in the generation of adakites, from the andean Austral Volcanic Zone, *Contrib. Mineral. Petrol.*, *123*, 263–281, 1996.
Sturm, M. E., E. M. Klein, D. W. Graham, and J. Karsten, Age constraints on crustal recycling to the mantle beneath the southern Chile Ridge: He-Pb-Sr-Nd isotope systematics, *J. Geophys. Res.*, *104*, 5097–5114, 1999.
Sun, S. S., and W. F. McDonough, Chemical and isotopic systematics of oceanic basalts: Implications for mantle composition and processes, in *Magmatism in the Ocean Basins*, edited by A. D. Saunders and M. J. Norry, *Geol. Soc. Spec. Publ.*, *42*, 313–345, 1989.
Tatsumi, Y., Geochemical modeling of partial melting of subducting sediments and subsequent melt-mantle interaction: Generation of high-Mg andesites in the Setouchi volcanic belt, southern Japan, *Geology*, *29*, 323–326, 2001.
Tebbens, S. F., S. C. Cande, L. Kovacs, J. C. Parra, J. L. LaBrecque, and H. Vergara, The Chile ridge: A tectonic framework, *J. Geophys. Res.*, *102*, 12,035–12,059, 1997.
Thorkelson, D. J., Subduction of diverging plates and the principles of slab window formation, *Tectonophysics*, *255*, 47–63, 1996.

N. Arnaud and H. Martin, UMR 6524 Magmas et Volcans, Université Blaise Pascal, 5, rue Kessler, F-63038 Clermont-Ferrand Cedex, France. (arnaud@opgc.univ-bpclermont.fr; H.Martin@opgc.univ-bpclermont.fr)

J. Bourgois, Centre National de la Recherche Scientifique, Université Pierre et Marie Curie, Boîte 119, 4, place Jussieu, F-75252 Paris Cedex 05, France. (bourgois@ccr.jussieu.fr)

J. Cotten, Y. Lagabrielle, and R. C. Maury, UMR 6538 Domaines océaniques, Université de Bretagne Occidentale, Institut Universitaire Européen de la Mer, Place Nicolas Copernic, F-29280 Plouzané, France. (Jo.Cotten@univ-brest.fr; Yves.Lagabrielle@univ-brest.fr; Rene.Maury@univ-brest.fr)

S. Fourcade, UMR 6118 Géosciences Rennes, Université de Rennes I, Avenue du Général Leclerc, F-35042 Rennes Cedex, France. (Serge.Fourcade@univ-rennes1.fr)

C. Guivel, UMR 6112 Laboratoire de Planétologie et Géodynamique, Universite de Nantes, 2 rue de la Houssiniere, BP 92208, F-44322 Nantes Cedex 3, France. (christelle.guivel@chimie.univ-nantes.fr)